Case Studies in Chemical and Environmental Engineering 8 (2023) 100428

Contents lists available at ScienceDirect

Case Studies in Chemical and Environmental Engineering

journal homepage: www.sciencedirect.com/journal/case-studies-in-chemical-and-environmental-engineering

Case Report

Aluminum oxide nano porous: Synthesis, properties, and applications

Ahmed Mahdi Rheima [a], Zainab sabri Abbas [b], Mustafa M. Kadhim [c], Srwa Hashim Mohammed [d], Dheyaa Yahaia Alhameedi [e], Fadhil A. Rasen [f], Alaa dhari jawad al-bayati [g], Montather F. Ramadan [h], Zainab Talib Abed [i], Asala Salam Jaber [j], Safa K. Hachim [k,l], Farah K. Ali [m], Zaid H. Mahmoud [n], Ehsan Kianfar [o,p,q,*]

[a] *Department of Chemistry, College of Science, Mustansiriyah University, Baghdad, Iraq*
[b] *Wasit University, College of Science, Department of Chemistry, Iraq*
[c] *Medical Laboratory Techniques Department, Al-Farahidi University, Baghdad 10022, Iraq*
[d] *Chemistry Department, College of Education, University of Garmian, Kalar, Iraq*
[e] *Department of Anesthesia, College of Health & Medical Technology, Sawa University, Almuthana, Iraq*
[f] *Department of Medical Engineering/ Al-Esraa University College, Baghdad, Iraq*
[g] *Department of Chemical Engineering and Petroleum Industries, Al-Mustaqbal University College, Hilla, 51001, Iraq*
[h] *College of Dentistry, Al-Ayen University, Thi-Qar, Iraq*
[i] *College of Pharmacy, The University of Mashreq, 10021 Baghdad, Iraq*
[j] *Department of Pharmacy, Mazaya University College, Thi-Qar, Iraq*
[k] *College of Technical Engineering, The Islamic, University, Najaf, Iraq*
[l] *Department of Medical Laboratory, College of Health and Medical Technology, National University of Science and Technology, Thi-Qar, 64001, Iraq*
[m] *Medical Laboratory Techniques Department, Al-Turath University College, Baghdad, Iraq*
[n] *University of Diyala, College of Sciences, Chemistry Department, Iraq*
[o] *Mechanical Engineering Department, Faculty of Engineering and Pure Sciences Istanbul Medeniyet University, Istanbul, Turkey*
[p] *Young Researchers and Elite Club, Gachsaran Branch, Islamic Azad University, Gachsaran, Iran*
[q] *Department of Chemical Engineering, Arak Branch, Islamic Azad University, Arak, Iran*

ARTICLE INFO

Keywords:
Aluminum oxide nanoporous
Nanostructures
Porous metal oxide
Anodic aluminum oxide
High-density parallel nonporous
Porous alumina structure

ABSTRACT

in recent years, most researchers are trying to seek out and develop effective and comparatively simple methods for producing nanostructures. In this regard, the methods of manufacturing self-regulated nanostructures with alternating arrays are given special attention. The anodization, which ends up within the formation of a porous metal oxide layer consisting of an everyday array of nanoporous, is one such method. The numerous applications of aluminum, research on the anodization has focused more on this metal. Anodic corundum may be a key sample material for creating nanostructures like nanowires, nanotubes. The anodic aluminum, which ends within the formation of porous alumina samples, is comparatively easy and ultimately leads to an array of high-density parallel nanoporous. During this paper, the final structure of porous anoxic alumina further because the growth mechanism of this layer within the presence of electrical field and therefore Penetration of Electrolyte species into the oxide layer, furthermore as explaining the expansion mechanism of porous oxide layer in steady state and hexagonal plasma membrane structure. Affecting the geometric parameters of the porous alumina structure like the pore diameter, the interpore distance, the wall thickness, and also Thickness of the Barrier Layer are discussed.

1. Introduction

Anodization is an anodic electrochemical process accustomed increase the thickness of the oxide layer that forms naturally surface metals. This process was first used on an industrial scale in 1923; it then expanded rapidly and was first performed in 1927 by Grower and O'Brien on vitriol electrolytes [1–7]. The anodization has many applications within the production of dielectric layers for the manufacture of electrolytic capacitors, sensors, and optical instruments. The resistance of anodic layers against corrosion and abrasion, likewise providing an

* Corresponding author. Mechanical Engineering Department, Faculty of Engineering and Pure Sciences Istanbul Medeniyet University, Istanbul, Turkey ,
E-mail addresses: ehsankianfar775@gmail.com, ehsan_kianfar2010@yahoo.com (E. Kianfar).

https://doi.org/10.1016/j.cscee.2023.100428
Received 3 June 2023; Received in revised form 15 July 2023; Accepted 23 July 2023
Available online 5 August 2023

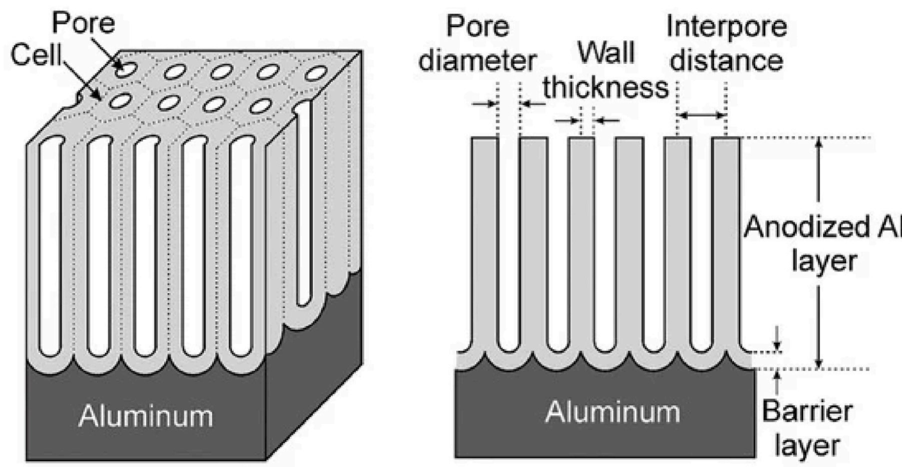

Fig. 1. (a) Structure Porous Anodic Alumina, (b) Cross Section anodization Layer [1].

appropriate substrate for colored and adhesive primers on metal surfaces, has made the anodization additionally to industrial applications, in fields like architecture [8–12]. Metal surface anodization changes surface texture changes the crystal structure of the metal near the surface [13–16]. The formation of a porous oxide layer in electrolytes with very strong acidic properties like acid, Ethane dioic acid has been reported; This layer is partially soluble [17–22]. In porous anoxic alumina, the expansion of the layer is the local Dissolution of Oxide, which eventually Results from the formation of holes within the oxide layer [23–28]. The expansion of the anoxic alumina layer at steady-state results from the interaction of two competing processes, which occur simultaneously [29–35]. One of these processes is the dissolution oxide layer at the top of the cavities at the interface between the oxide layer and therefore the electrolyte, and therefore the other is the formation of the oxide at the interface between the oxide and metal layers [36–41]. The Aim study analyze the link between anodization conditions, like applied potential, temperature, electrolyte concentration, and therefore the geometric properties of porous alumina structures. In other words, by changing the anodization conditions, the geometric parameters of porous alumina will be controlled and thus the required structure is often achieved [42–47].

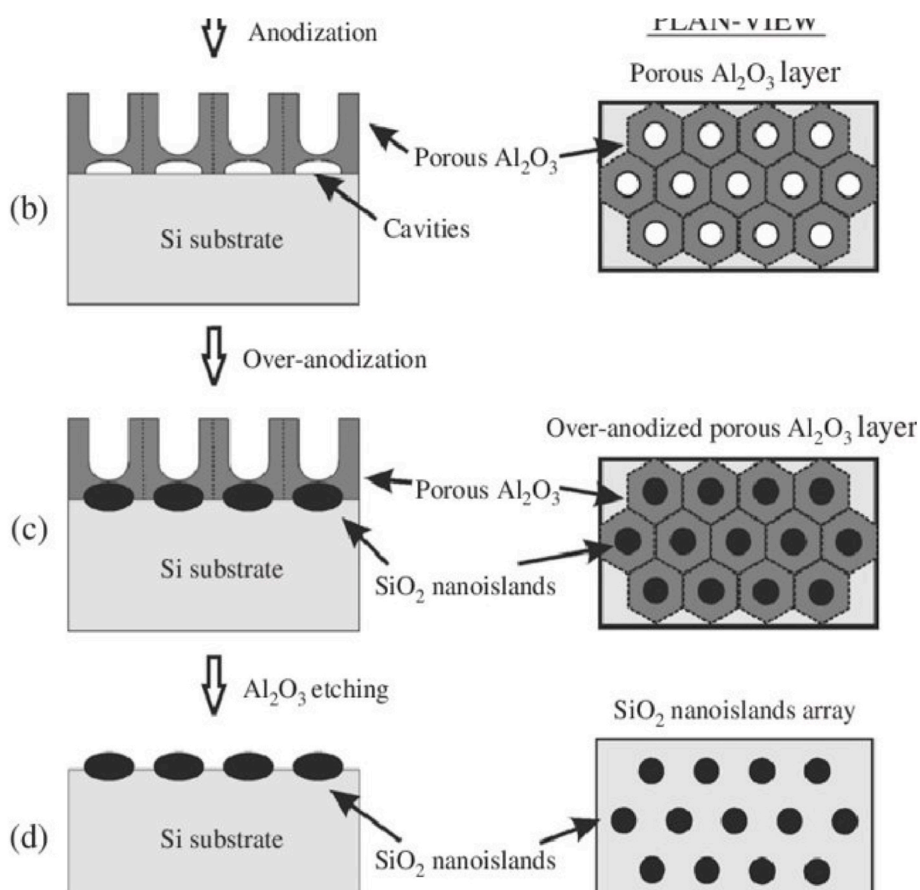

Fig. 2. The Increase of SiO_2 Nano islands on silicon using a porous anodic alumina template is depicted schematically [2].

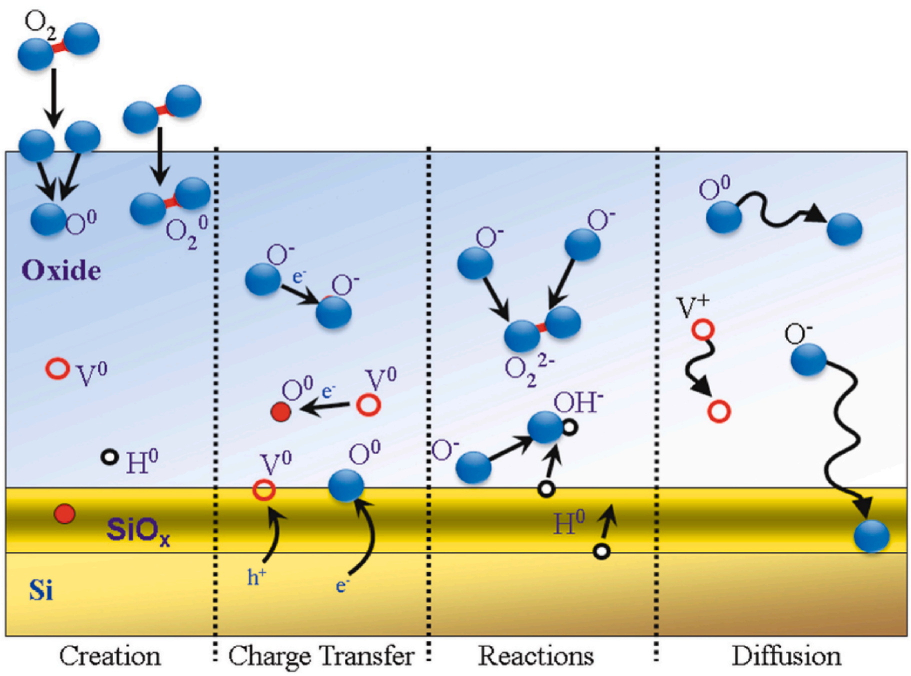

Fig. 3. The formation of O^{-2} and OH^- ions at the oxide and electrolyte border, as a result of the reaction of water with absorbed O^{-4} ions from the source [4].

2. Structure of porous anodic alumina

The formation of alumina thin film isn't only associated with the anodization and is even achieved in an exceedingly simple oxidation process. But what has attracted plenty of attention is the special nature of the porous layer of aluminum oxide, which is created under certain conditions and has many applications in nanotechnology [48–53]. The structure of the self-assembled porous anodic alumina layer, formed under anodic aluminum, is described as an array of tightly packed hexagonal cells, each cavity centered within the center of a cell [54–60]. The porous alumina coating is illustrated schematically in Fig. 1. Various theories are suggested for the formation of nano porous within the alumina crust; nevertheless, what's clear is that the oxide coating grows at the tip of the cavities, on the metal-oxides bound substrates. In this way, the present substance on the surface is converted into a shield layer, which is followed by a porous oxide layer [61–65]. A skinny and compact barrier layer dissolve on the electrolyte's joint surface and also the cavity's rim during the formation of porous oxide, and a brand-new barrier layer forms on the oxides and metals joint s surfaces. Within the steady-state of layer growth, a dynamic equilibrium is made between the speed of layer growth and therefore the rate of dissolution by the ground [66–72]. Because the oxide layer grows steady state, the anode current density remains almost unchanged at constant potential (or anode potential under constant current density). The cylindrical part that appears at the cross-section of the cavities is the result of growth within the steady-state [73–80]. The standardized pore diameter may be easily managed by changing the anodization conditions from some nanometers to some 100 nm [81–85].

3. Mechanism of growth of porous oxide layer in the presence field

The structure of porous alumina begins and extends from the physical phenomenon that emerges at the beginning of anodization on the aluminum surface. Solid ionic conduction induces physical phenomenon formation. This happens within the presence of a constant-power field; the magnitude of the electrical field is defined because of the ratio potential along with the barrier layer thickness [86–90]. As seen in Fig. 2, the barrier oxide layer extends evenly over the surface with a standardized field distribution controlled by a continuing field [91–96]. The rough surface of the aluminum becomes smoother as a result test of uniform growth. Local changes in field pressure, on the opposite hand, may manifest themselves on the surface as defects, impurities, or surface features like subgrain borders, ridges, and troughs [97–105]. Increased field dissolution to the oxide layer and native thickening porous layer result from this non-uniform flow distribution (Fig. 2-b). A Joule local heating is followed by more current above the metal ridges, leading to a thicker barrier oxide layer [106–114]. The bottom breakdown of the oxide layer, on the opposite hand, helps to flatten the oxide-metal interface. This local heat increases the sphere breakdown of the oxide at the cavities' ends, increasing the current's local density. This mechanism continues because the local current density rises, causing the oxide within the lower part of the cavities to dissolve. The oxide layer that grows on the ridges (on the surface's deficient points) is vulnerable to high local pressure [115–123]. This causes consecutive cracks within the oxide layer, but these cracks suddenly strengthen at high local current densities (Fig. 2-c, 2-d). Cracking-healing events are typical where aluminum is employed as a base and oxide layer walls are built above the defective areas. This enables a part of the wall to crumble, increasing the spherical curvature of the cavities on the metal and oxide joint surface (Fig. 2-e). The flow is localized within the thinner section of the film at the top of the following cavity, leading to preferential development of the oxide over the deficient areas and thickening of the barrier layer. Consequence, event cavities begin the initial cavil ties to preserve a uniform area. The steady-state of cavity growth happens because the curvature of the oxide layer at the metal-oxide joint surface increases enough and therefore the intersection of the hemispherical regions occurs [124–128].

4. Permeability anions

Anions' permeability to the structure of the anodization oxide layer is extremely influenced by the kind of oxide layer produced [129–135]. The penetrating anions within the porous oxide layer are much greater than the boundary oxide layer's penetrating anions. The expansion of the oxide happens concurrently at the oxide-metal boundary and at the electrolyte oxide boundary during the formation of a barrier oxide layer within the steady-state, which is the migration of $Al^{3+}$and HO^-/O^{-2} ions in opposite directions. Al^{3+} ions, on the opposite hand, are directly introduced into the electrolyte solution and play no part within the forming of the oxide layer [136–143]. The amorphous oxide film is built he aluminum. The penetration of anions into the oxide layer at the underside of the cavities, which may be a direct result of electrolyte species migration, is required to develop a layer of porous alumina. Since electrolyte kinds may be positively, negatively, or neutrally charged, they will either because immobile on the oxide surface or migrate at or specific rate, which varies counting on electrolyte [144–150]. PO_4^{3-}, SO_4^{2-}, oxalate anions, for instance, migrate into the oxide layer, while chromate anions migrate outward [151–156]. The oxide layer grows only at the interface between the oxide and therefore the metal during the formation of porous alumina, and also the anions move through the barrier layer because the presence of an electrical field shanks the circular structure of the underside of the openings, the electrical field within the barrier layer isn't uniform [100]. The electrical field at the underside of the cavities, where the oxide meets the electrolyte, is far stronger than the electrical field at the underside of the cell, where the oxide meets the metal [157–163]. As a result, the electrolyte anions have a straightforward time managing to infiltrate. The longer the oxide walls are subjected to the acid's aggressive penetration; the more anions penetrate into the porous alumina base [164–170].

5. Anodization, steady growth of the porous oxide layer

The following reactions release OH^- ions in the electrolyte solution: quick decomposition of water or cathode reduction of dissolved water and oxygen:

$$H_2O + 2e^- \rightarrow 2OH^- + H_2 \quad (1)$$

$$O_2 + 2H_2O + 4e^- \rightarrow^- 4OH \quad (2)$$

O^{-2} ions, on the other hand, are formed at the oxide-electrolyte interface due to the loss of oxygen vacancy, which contributes to the adsorption of OH- ions [171–176], either in the simple decomposition of water or in the reaction of water with the adsorbed electrolyte ions. Fig. 3 depicts the mechanism of producing O^{-2} and O^{H-} ions at the interface between the oxide and the electrolyte.

As aluminum is anodization in an acid electrolyte, the following reactions occur, resulting in the formation of an amorphous oxide layer:

$$2Al^{\ 3+} + 3H_2O \rightarrow Al_2O_3 + 6H + +^- 6e \quad (3)$$

$$2Al + 6OH^- \rightarrow Al_2O_3 + 3H_2O^- + 3e \quad (4)$$

$$2Al + 3O^{2-} \rightarrow Al_2O_3^- + 6e \quad (5)$$

In anodization flow, the following reaction is important:

$$Al \rightarrow Al^{-\ 3+} + 3e \quad (6)$$

For the anodization of aluminum in different electrolytes, the movement of oxygen near the oxide-metal boundary has been recorded [177–184]. The following are some of the reactions:

$2H_2O \rightarrow O_2 + 4H\text{-}+ 4e$ (7)

$$4OH\text{-}\rightarrow 2H_2O +^- O_2 + 4e \quad (8)$$

$$2O^{2-} \rightarrow^- O^2 + 4e \quad (9)$$

Due to the presence of impurities, the production of oxygen bubbles within the anodization alumina, according to reaction (9) near the boundary of the oxide and metal substrate, will begin [185–192]. It's also been proposed that the development of the porous alumina layer is linked to oxygen transport. The presence of electrolyte anions, which are vulnerable to oxidation, complicates the anodic process:

$$2SO_4^{2-} \rightarrow^- 2SO_8^{2-} + 2e \quad (10)$$

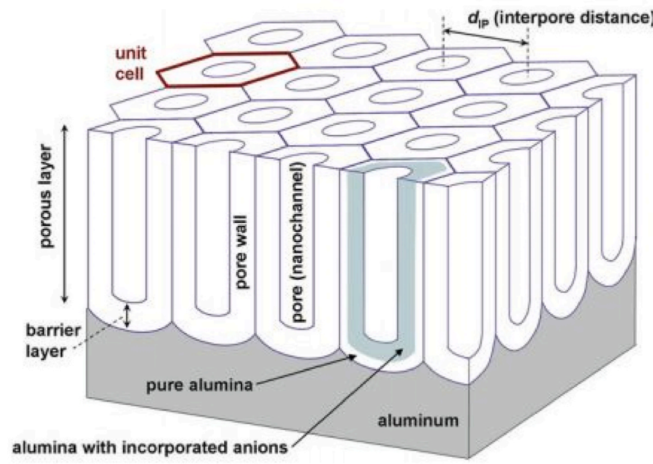

Fig. 4. The ideal structure of the porous alumina layer on the aluminum substrate [7].

Cavities are formed as a result of thermal dissolution caused by Presence of an oxide layer field at the cavity's end. The expansion of the oxide layer in typical acid electrolytes, like vitriol, oxygen acid, and acid, occurs primarily at the Interface between the oxide and therefore the metal. The movement of oxygen-carrying ions (O^{-2} and OH^-) from electrolyte solution into the oxide layer induces expansion of porous alumina at the underside of the cavities. At Interface between the oxide layer and also the electrolyte, Al^{3+}ions that are progressing through the oxide layer are forced into the electrolyte solution. In fact, metal ion migration into electrolyte solution could be a required condition for the forming of a porous oxide layer, since when these ions meet the common surface of the oxide layer and also an electrolyte, they permit the barrier layer to expand and thus contribute to the formation of the oxide layer [193–200].

Just a little portion of the Al^{3+}ion flux at the oxide/metal and oxide/electrolyte interfaces, however, contributes to the forming of the oxide layer. Electrolyte ions can also move through barrier layer and interact within the formation of metal oxide compounds. Dissolution of the oxide layer at the underside of the cavities is caused by the local increase of the sphere at the favored boundary of the oxide and therefore the metal for the event of the solid-state of porous oxide [201–205]. The complex equilibrium between the oxide field dissolution rate and also the oxide-forming rate increases the expansion rate of the oxide at the interface between oxide and therefore metal because the field dissolution rate of the oxide layer is increased. The polarization of Al–O bonds initiates field breakdown of the oxide, by separation of Al^{3+}ions from oxide structure [206–214]. It's also simpler to tell apart Al^{3+}ions within the presence of the bottom [215–221].

6. Cell wall structure

Structure of the cell membrane the penetration of electrolyte Kinds into oxide walls determines properties of porous alumina layer formed during the anodization. Furthermore, anions' penetration affects the mechanical properties of the anodization alumina layer, like stability, stiffness, and abrasion resistance [222–230]. Anodization factors like anodization potential and temperature influence the sum of infiltrating organisms and their distribution. Fig. 4 illustrates the twin arrangement of the cell membrane.

Thomson et al. proposed that this structure is created from two layers, one among almost pure alumina and therefore the other with electrolyte penetration anions [231–236]. Reckoning on the shape of acid used, the thickness of the inner layer increases as follows:

$$H_2SO_4 < C_2H_2O_4 < H_3PO_4 < H_2CrO_4 \quad (11)$$

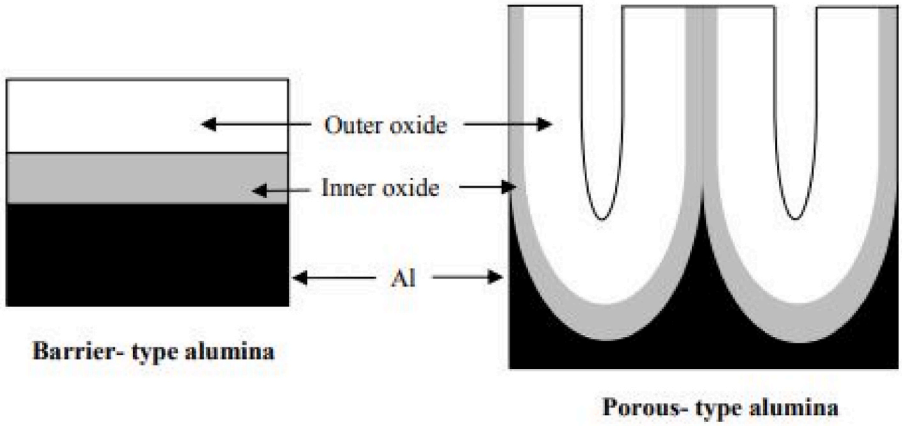

Fig. 5. Vacancies in the structure of porous Anodic alumina [8].

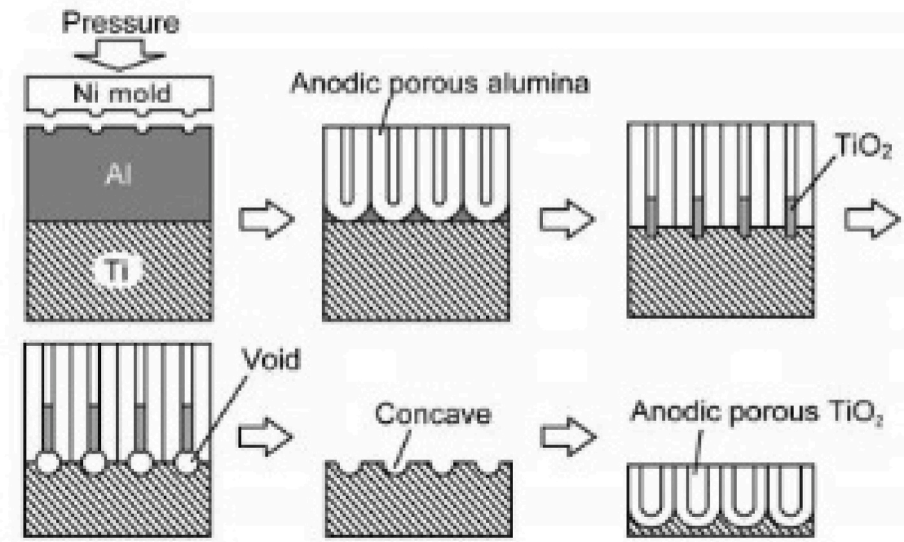

Fig. 6. Steps of formation of voids in the structure of porous anodic [9].

Table 1
Set of nanowires made of metals with their deposition techniques and investigated properties [286–290].

Metal or alloy	Deposition technique	Investigated properties/applications/remarks
Al	Pulse electrodeposition	–
Al	Surface redox reaction (cementation)	–
Ag	DC electrodeposition	–
Ag	AC electrodeposition	Antibacterial properties
Ag	AC electrodeposition	–
Ag	AC electrodeposition	Plasmonic properties were strongly related to the NW diameter
Ag	DC electrodeposition	Diameter-modulated NWs
Ag	Solid state reduction	–
Ag–Au	AC electrodeposition	UV–vis absorption spectra
Au	DC electrodeposition	Optical properties
Au	AC electrodeposition	DNA arranging on the Au NWs surface
Au	DC electrodeposition	–
Au	AC and subsequent DC electrodeposition	–
Au	DC electrodeposition	Diameter-modulated porous NWs
Au	DC electrodeposition	Y-branched NWs

Moving over the membrane and into the cavity, there's a transition from a solid to a jelly-like state. For oil of vitriol, ethane dioic acid, and oxygen acid electrolytes, the thickness ratio of the inner layer to the outer layer is 0.05, 0.1, and 0.5, respectively [11]. The cell wall's triangular shape, as seen in Figs. 5 and 6, was recently stated [12]. Electrolyte species, mostly protons, and anions are impurities within the outer and middle layers. Anions and protons are abundant within the outer layer, while anions dominate the center layer. The cell wall's triangular shape, as seen in Figs. 5 and 6, was recently stated [12]. Electrolyte species, mostly protons, and anions, are impurities within the outer and middle layers. Anions and protons are abundant within the outer layer, while anions dominate the center layer. Oil of vitriol electrolytes produces porous oxide layers that are practically dry [14]. Within the porous alumina structure, voids are found at the information of the aluminum protrusions, at the interface between the metal and also the oxide, within the inner layer of the cell walls, these voids, which are formed by the passage of oxygen, are thought to be created to survive the strain within the layer [237–240]. With increasing anodization potential, the quantity of voids created within the porous oxide layer increases [241–246].

To form nanowires (high-aspect ratio 1D nanostructures), AAO template has to be thick enough and experimental procedure has to provide relatively large charge during the electrodeposition (Table 1).

DC electrodeposition, AC electrodeposition, and pulse electrodeposition are used to obtain highly ordered arrays of nanowires made of Al, Ag, Ag–Au, Au, Bi, Co, and its alloys, Cu, Fe, and its alloys, Ni, and its alloys, Sn, Pd, and Pt (Table 1).

7. Geometric parameters characteristic of nano porous anodic alumina

Regular nanostructures, often with parameters such as pore diameter, interpose distance, wall thickness, barrier layer thickness, porosity, pore density, and thickness of the oxide layer is described [247–252].

7.1. Pore diameter

In general, the pore diameter of porous anodic alumina structures anodization linearly with probability, and the constant of proportionality in this respect, p is equal to 9.0 nm volts for soft anodized and 0.4 nm V for hard anodized [253–257]:

$$Dp = \lambda p.\ U \tag{12}$$

The hole diameter (nm) is represented by p, and also the anode potential is represented by U (V). Electrolyte shift has no effect on the complete diameter's dependency on the anodization potential. Researchers often use the terms outer layer for areas near the oxide layer surface and inner layer for areas near the top of cavities when defining the composition of porous anodic alumina [148–151]. The pore diameter of the outer oxide layer doesn't change substantially with time at steady state; the greater diameter of the pores at the surface of the oxide layer is that the product of early development and irregularity of the porous alumina layer within the early stages of growth [8,10,15]. The diameter of the holes is clearly sick with the electrolyte temperature and hydrodynamic conditions within the electrochemical cell. A rise within the speed of chemical dissolution of the outer oxide layer is predicted when anodization at higher temperatures (near room temperature), particularly in electrolytes with high acidity [258–262]. Reducing the stirring speed of the electrolyte during anodization under constant potential, on the choice hand, increases the local temperature of the inner oxide layer and hence this density [18,263–268]. As a result, chemical dissolution of the inner oxide layer and electrochemical forming of the anodic oxide layer happens more quickly, and also the pore diameter increases.

7.2. Distance between holes

It is generally accepted that the distance between holes in a porous anodic alumina structure is linearly related to the growth potential of the oxide layer, and the proportionality constant, λc, is approximately 2.5 nm for soft anodization and 1.5–2 nm for hard anodization. Is in nanometers per volt [19]:

$$Dc = \lambda c.\ U \tag{13}$$

The distance between the cavities can be partially, at constant potential, dependent on the anode temperature or independent of it. If anodization is performed in the presence of oxalic acid as the electrolyte, the distance between the cavities will not be temperature dependent [20]. Conversely, if the anodized electrolyte is sulfuric acid, the distance between the cavities will be temperature dependent [21]. Research by O'Sullivan and Wood has shown that increasing the electrolyte concentration reduces the distance between cavities [2]. They performed anodization on sulfuric acid electrolyte at constant current density and observed that increasing the anodization temperature also increased the distance between the cavities by increasing the electrolyte concentration.

7.3. Wall thickness

According to the research of O'Sullivan and Wood, the hole diameter for anodization under constant potential is calculated from the following equation [2]:

$$Dp = Dc - 2W \tag{14}$$

Where Dp is the pore diameter, Dc is the distance between the cavities and W is the wall thickness. In this way, the wall thickness can be calculated from the above equation, as follows:

$$W = (Dc - Dp)\ /\ 2 \tag{15}$$

They also showed that for anodization in phosphoric acid, wall thickness was linearly related to the thickness of the barrier layer:

$$W = 0.71B \tag{16}$$

$$B \approx Dc\ /\ 2 \tag{17}$$

They reported that the ratio between the wall thickness and the thickness of the barrier layer at the anode in the oxalic acid electrolyte varies slightly in the voltage range of 5–40 V. For voltages between 5 and 20 V, this proportionality constant is 0.66, which as the voltage rises to 40 V, this value also increases slowly and eventually reaches 0.89 [2,106,107,152–156].

7.4. Thickness of the barrier layer

The barrier layer forms at the top of the cavities during the anodization of aluminum. It's a really thin, thick, flexible dielectric layer. This coating is analogous to the oxide layer that normally occurs within the atmosphere therein it only allows current to circulate if its composition includes defects. The electrochemical accumulation of metals into the cavities is nearly unlikely because of the inclusion of this lightweight membrane sheet at the top of the cavities. Given this restriction, the thickness of the barrier layer is very important, and it'll be a deciding think about the next applications of anodized Nano pores [157–161,269–272]. The anodization ability defines how dense the barrier layer. Changes within the thickness of the barrier layer are identified in some studies as a result of changes in electrolyte concentration [32–34,108–110,273–280]. The researchers inferred from their experimental findings that the thickness of the barrier layer varies with anode voltage counting on whether the anode was performed within the constant potential or constant current density regime [35,36,281–283]. Within the constant potential regime, increasing anode temperature ends up in a decrease within the thickness of the boundary layer; within the constant current regime, the alternative relationship is found. In anodization at constant potential, decreasing the thickness of the barrier sheet, and anodization at constant current density, increasing the concentration of oxyacid at constant temperature increases this amount [37-40,285-285]. The anodization rate, BU (ratio between barrier layer thickness and anodization potential), up to 1 nm/volt, is shown by the diagonal line of the line during this diagram. In general, the anodization rate is incredibly the same as 1 nm for various electrolytes and over the complete anodization potential spectrum. This result suggests a general relationship between anodization rate and anodization potential. For the most effective self-regulated anodization conditions, Nielsch et al. suggested the subsequent relationship for the barrier layer thickness and therefore the distance between the cavities [3,117–120], which ends in 10% nanostructure porosity and therefore the arrangement of six full Nano porous cells: The thickness of the physical phenomenon is denoted by the letter B.

7.5. Porosity

Porosity is defined as the ratio of the surface occupied by cavities to

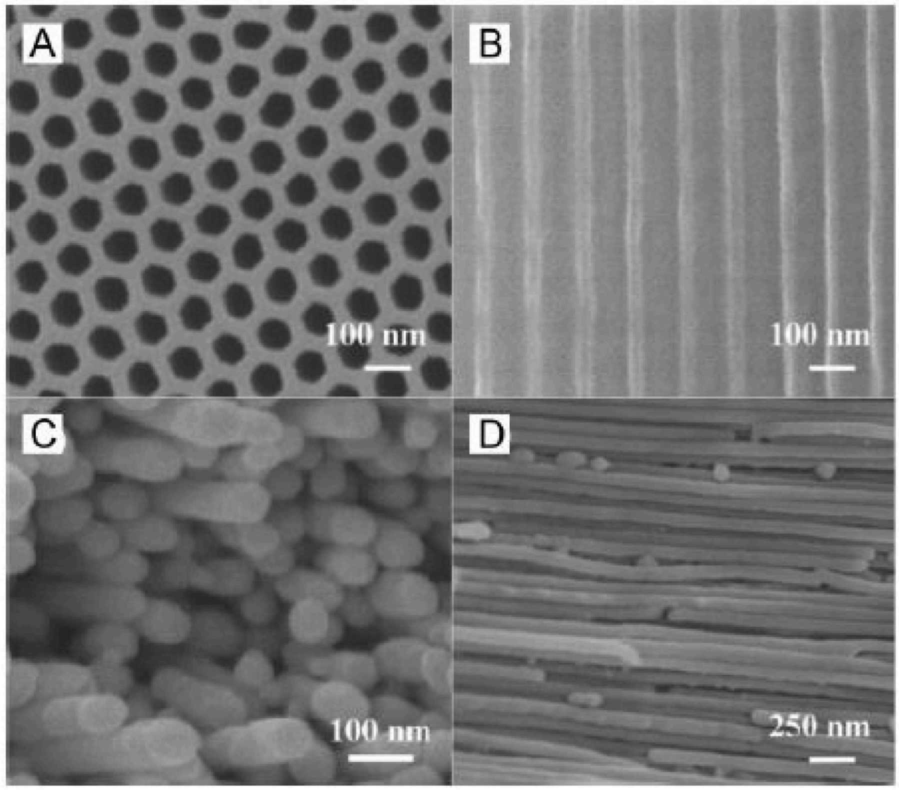

Fig. 7. SEM images of the surface (A), the cross-sectional views (B) of the ordered porous anodic alumina template, the top image of as-prepared 70 nm AgI nanowires after partial removal of AAO (C), and the cross-sectional view of AgI nanowires after complete removal of AAO (D) [1].

the total surface area of the porous oxide layer. For a regular hexagon with a hole in the center, the porosity formula is written as follows:

$$\alpha = \text{Spores} / S = Sp / Sh \quad (18)$$

Assume that each single hole is a complete circle. So for Sp and Sh we have:

$$S_p = \pi (D_p / 2)^2 \quad (19)$$

$$Sh = (\sqrt{3} / 2)\, Dc^2 \quad (20)$$

By placing equations (19) and (20) in equation (18), the following expression is obtained to calculate the nanostructured porosity consisting of an array of six cell phones:

$$\alpha = (\pi / 2\sqrt{3})\, (Dp / Dc) \quad (21)$$

The growth rate of the oxide layer and its chemical dissolution rate within the acid electrolyte, furthermore as anodization conditions like electrolyte form, electrolyte concentration, potential, and anodization temperature, all influence the porosity of nanostructures created with anodization aluminum. The anodization potential and pH of the electrolyte used are the foremost significant variables in assessing the porosity of anodic alumina nanostructure. With increasing anodization potential in acid and Ethanedioic acid, an exponential decline in porosity has been observed [41,121–123]. Porosity nanostructures will influence with anodization time, as predicted. In tetra borate and oxyacid, prolonged anodization time often leads to increased nanostructured porosity [42,43,124–126].

7.6. Cavity density

High-order nanomaterials with a structure composed of compact clusters of Nano pores or nanotubes are of significant importance in the microelectronics industry. Porous anodic alumina was chosen because of the hexagonal symmetry of the cells. The number of cavities that develop during anodization is one of the most significant properties of porous alumina since nanopores have the highest density and compaction. The density of cavities is defined as the total number of cavities occupying a 1cm^2 region for the distribution of six cell phones in nanostructures [44,45,127–130]. The following is the suggested relationship for measuring the density of cavities:

$$n = 10^{14} / P_h = (2 \times 10^{14} / \sqrt{3}).\, D_c^2 \quad (22)$$

The pH is the surface area of a single six-cell phone (nm^2) and the Dc is nanometers. By inserting Dc from the relation Dc = λc. U, we will have:

$$n = (2 \times 10^{14} / \sqrt{3}\, \lambda_c^2 \times U^2) \approx 18.475 \times 10^{14} / U^2 \quad (23)$$

Increasing the anodization potential or the distance between the cavities reduces the amount of cavities formed in the porous alumina structure [7], as shown by Equations (22) and (23).

7.7. Volume expansion

The Pilling-Bosworth Ratio is the volume expansion of porous anodic alumina (R) (PBR). The amount of aluminum oxide formed in the anodization process divided by the volume of aluminum consumed is known as volume expansion:

$$RV\ \text{Alumina} / V\ Al = M\ \text{Alumina}.\ d\ \text{Alumina} / M\ Al.\ d\ Al \quad (24)$$

(M)Alumina represents the molecular weight of aluminum oxide, (M) Al represents the atomic weight of aluminum, (d) Alumina represents the density of porous alumina (3.2gr/cm^3), and (d) Al represents the density of aluminum (2.7gr/cm3). PBR has a potential value of 1.6 for the formation of porous anodic alumina with a flow efficiency of 100%. Due to the utility below 100% of the flow, the experimental value

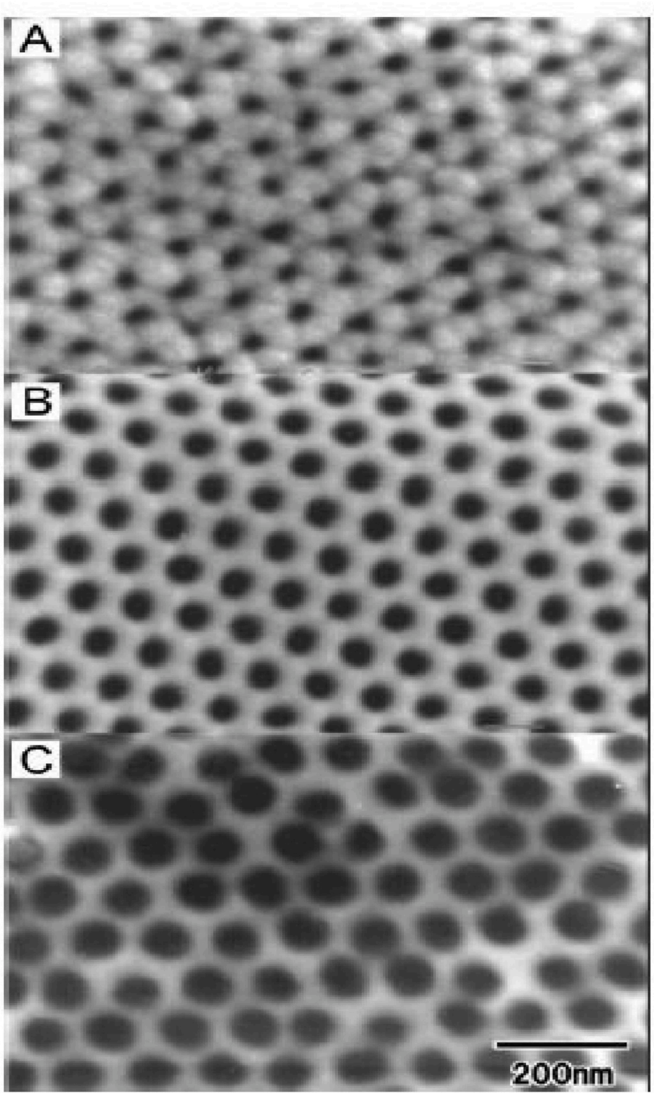

Fig. 8. SEM images of WO3 antidot arrays with different mean hole sizes: (A) 38 nm, (B) 53 nm, and (C) 65 nm fabricated by a two-step replication process employing negative-type PMMA templates. The PMMA templates have been prepared from highly ordered AAO membranes with different pore diameters [1].

of volumetric expansion differs significantly from the theoretical value and normally ranges from 0.9 to 1.6 [14].

8. Factors affecting the geometric parameters of porous alumina structure

Anodization conditions, which include electrolyte type, electrolyte density, anodization potential, temperature, electrolyte stirring, and anodization time, have a big effect on a range of porous anodic alumina structural parameters like pore diameter, pore spacing, pore density, and pore density [131–135,169–172]. The arrangement of cavities produced under different conditions with the identical magnification (Fig. 7).

8.1. Potential effect

The anodization potential is proportional to the gap between the cavities, because the potential rises, the interpore distance rises likewise. Figs. 10 and 11 precisely demonstrate this. It's worth noting that anodization capacity features a smaller impact on cavity diameter than it does on cavity spacing [46–48].

The Nano-cavity arrangement principle and structural properties of porous anodize alumina were investigated for anodized samples at different cell potentials from 100 to 200 V [291–295]. Two-stage anodization of aluminum was performed during a solution of 0.3 M H_3PO_4 or a methanol-water mixture. (1: 4 vol) at 0 a d −5 °C. Emission Scanning Electron Microscopes views of porous structures with images Fast Fourier Transform intensity profiles for anodized samples at 0.3 M H3PO4 at the bottom (100V) and highest (200V) anodization potentials are shown in Fig. 8, respectively [296–300]. Once again, an exquisite agreement is observed between the experimental fit constant and also the theoretical value for anodized samples in methanol-water mixture (1: 4 vol) [301–304]. These results indicate that the anodization of aluminum within the methanol-water system can cause porous structures with better pore arrangement. The particular proven fact that the porous anodize alumina films obtained with anodization aluminum in antacid show a fancy structure with sub-pores formed below the surface (clearly visible in Fig. 8), the common pore diameter isn't estimated. And potential impact analysis on pore diameter wasn't per.

8.2. Effect of electrolyte type

Each electrolyte has a specific anodization potential spectrum. Anodization with sulfuric acid electrolyte produces the greatest density of cavities, according to the evidence [49,136,137]. Anodization is an electrochemical process that can be applied to some metals. This process, depending on the nature of the electrolyte used, leads to the formation of two types of oxide and porous layers on the surface of metals [138–143,173–176]. When the anodization is performed in the presence of strong acids, the resulting oxide layer will be porous. In general, anodization is done in two ways: anodization with a guide template and self-organizing anodization. In anodization the metal, with a very high percentage of purity as anode and other metals such as aluminum, titanium, platinum, nickel and, sit in the cathode position and the nature of the electrolyte depends on the type of oxide layer and its properties such as hole diameter, distance It varies between cavities and cavity size. Cavity size (either average pore size or pore size distribution) is one of the properties of the material that is not well defined but is often the most useful and fundamental property of Nano process materials. The shape and size of the cavities are controlled by several independent variables, which leads to the distribution of the size and shape of the cavities, but in practice, these contents are never taken into account and the cavities are usually assumed to be narrow holes or cylinders [177–180]. This assumption leads to the definition of a specific parameter for size, which is the distance between the walls or the radius of the cylinder. The pore size distribution is often interpreted qualitatively to determine how regular material is, or in other words, how narrow the pore size distribution is.

8.3. Effect of electrolyte stirring

The anodization is critical and unquestionable. In fact, without stirring the electrolyte, the temperature at the top of the cavities rises dramatically [50]. Poor chilling can easily cause the breakdown of the oxide layer or anodic solution, especially at high currents (hard regime). Additionally, the electrolyte compositions at the underside of the cavities differ from the electrolyte bulk [50,51]. In general, by increasing the stirring speed of the electrolyte and decreasing its acid concentration, self-regulating growth of cavities occurs and better amounts of potential are often applied [181–183]. Electrolyte agitation is one of the important parameters within the geometry of the structure of porous alumina the diameter of the holes.

8.4. Effect of anodization temperature

As the anode temperature increases, the anode potential range

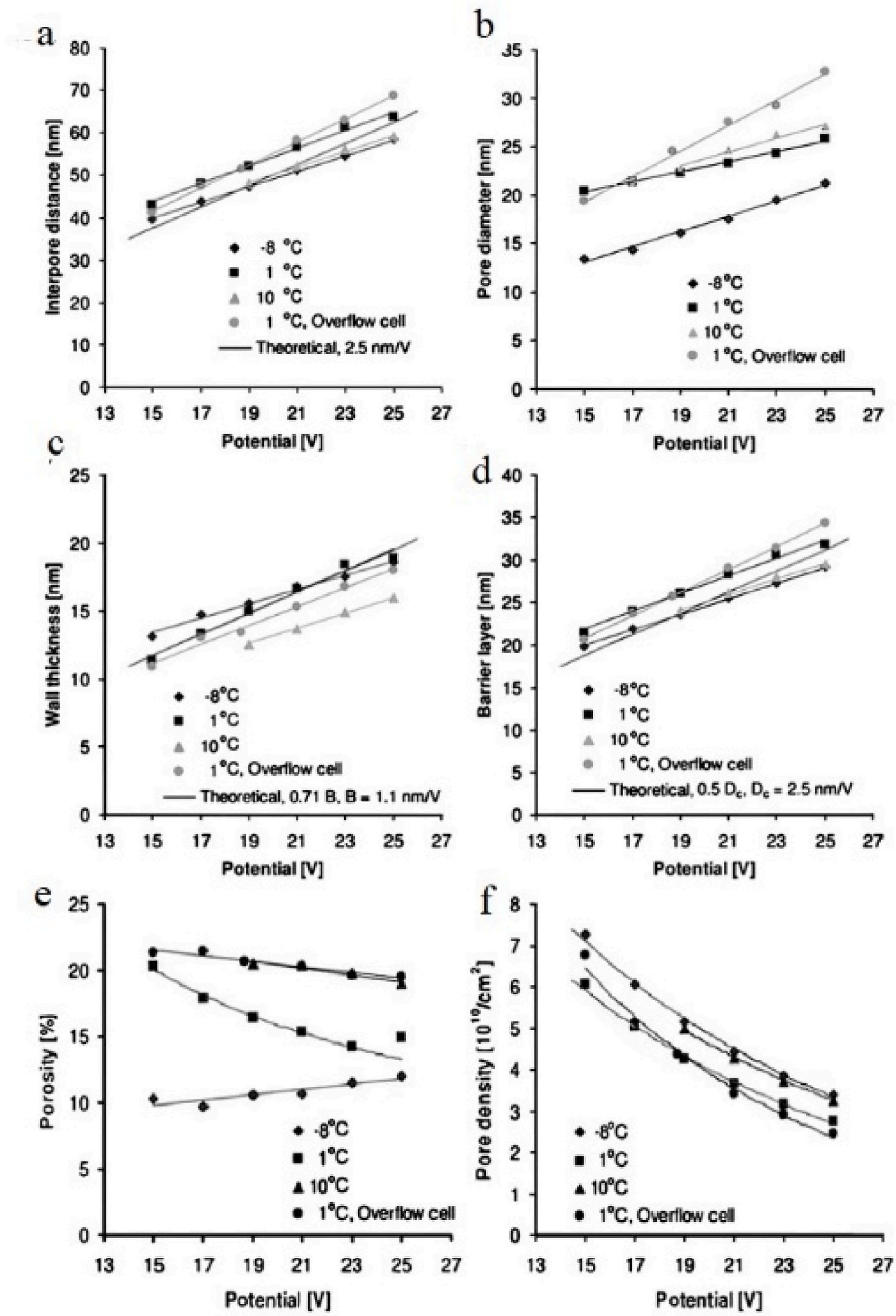

Fig. 9. The effect of anodization temperature, in terms of potential changes, on the parameters (a) the distance between cavities, (b) the pore diameter, (c) the wall thickness, (d) the thickness of the dam layer, (e) the porosity and (f) the density of the cavities; For example, anodized in 2.4 M sulfuric acid electrolyte [11].

decreases. At 10 °C, porous alumina only forms within the range of 17–25 V. Examination of experimental results shows that anodization temperature has little effect on changing the interpore distance and therefore the thickness of the barrier layer [2]; however, changes in cavity diameter and wall thickness are significant with changes in anodization temperature. In general, because the anode temperature increases, the pore diameter increases, and also the wall thickness decreases. The very cheap dissolution rate of the oxide layer occurs at −8 °C and therefore the smallest cavity produced is reported at the identical temperature. Similarly, the thinnest cell walls are observed at the best temperature studied. Anodization temperature also affects the porosity of the anodic alumina layer and also the cavity density [184–186]. The porosity of the corundum layer is between 10 and 20% within the whole potential range and for all studied temperatures. Fig. 9 shows the effect of anodization temperature on the gap between the cavities, the pore diameter, the wall thickness, and also the thickness of the barrier layer, the porosity, and also the density of the anodic alumina cavities. However, the analysis of the pore arrangement performed on the premise of FFT images doesn't provide a transparent answer about the effect. Fig. 9 shows that increasing the duration of both anodization steps improves the regularity of pore arrangement and uniformity of pore shapes. This can be attributed to the actual fact that within the two-step self--organized antonym anonymization of aluminum a giant extension of the first anodization step improves considerably the regularity of the array of Nano-periodic concave, consisting of a triangular lattice structure, on the aluminum substrate after the oxide layer removal [187–190]. The

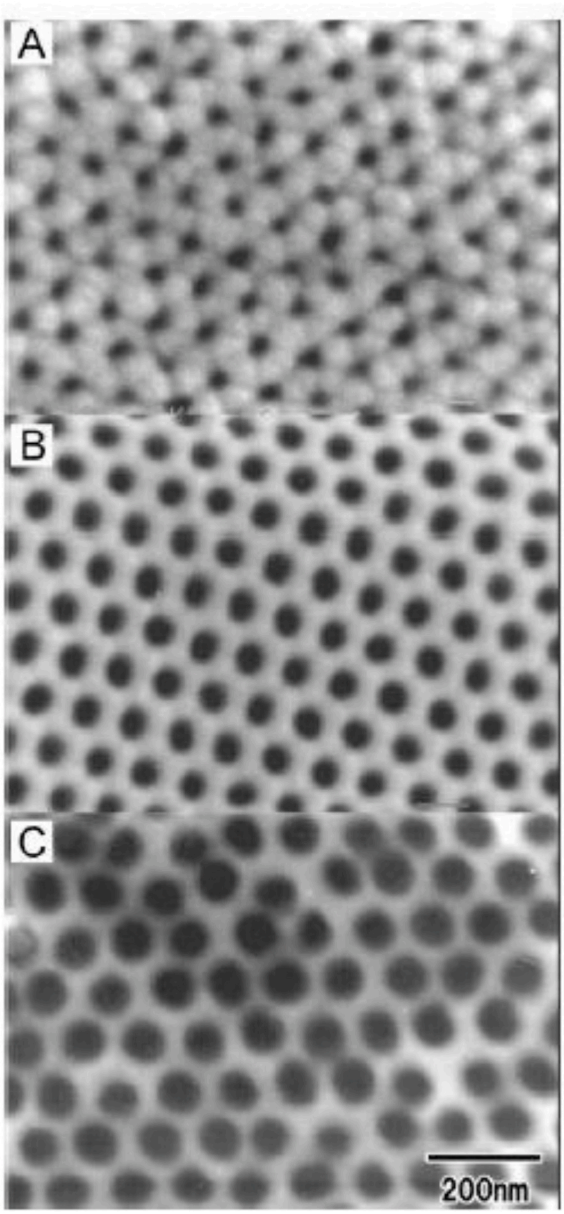

Fig. 10. SEM images of WO3 antidot arrays with different mean hole sizes: (A) 38 nm, (B) 53 nm, and (C) 65 nm fabricated by a two-step replication process employing negative-type PMMA templates. The PMMA templates have been prepared from highly ordered AAO membranes with different pore diameters [1].

periodic concave triangular features formed on the aluminum surface function nucleation sites for the formation of pores during the second anodization step. In consequence, the regularity of pore arrangement observed after the second anonymization is extremely improved.

8.5. Effect of anodization time

While anodization time influences the pore diameter, it's widely agreed that it's little effect on cell size [21,138]. The pore diameter increases because the anodization time increases; this process is caused not only by the chemical breakdown of the oxide layer, but also by the coalescence and forming of a solid wall [21]. The order of the cavities is additionally suffering from the anodization time; because the anode time in various electrolytes increases, the array of Nano pores becomes more uniform [17]. Furthermore, the number of cracks and dislocations within the porous alumina system reduces over time.

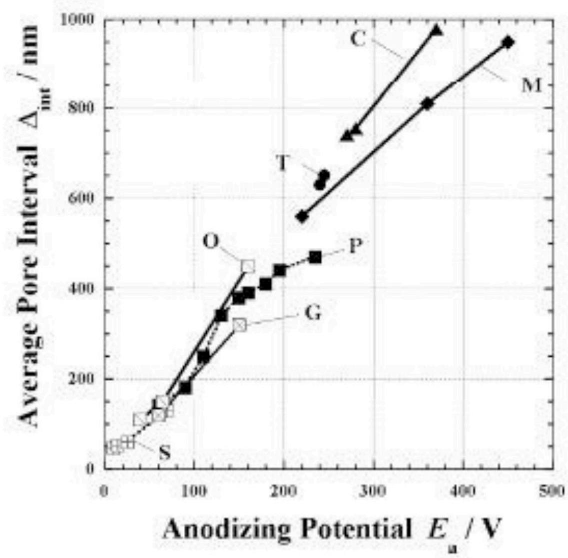

Fig. 11. Effect of anodization potential on the cavity distance for porous anodic alumina formed in different electrolytes. Dotted arrows are related to hard anodization in sulfuric acid, oxalic acid and phosphoric acid electrolytes [10].

9. Luminescent properties of anodic aluminum oxide

As it was mentioned above, during anodic oxide growth, positively polarized anode attracts negatively charged anions [284]. Next, the anions are being adsorbed on the oxide's surface and then incorporated into the AAO walls. Thus, anodic alumina poses anionic impurities in its walls. According to Rauf et al. [305], intensity of PL originating from F-centers can be also controlled. The worse the nanopores' arrangement, the more the defects, like F-centers present in the AAO walls. Therefore, the worse the nanopores' arrangement, the more intensive the PL from the F-centers. Both pore diameter and nanoporous array arrangement influence the PL of the AAO. Simultaneously, morphology and arrangement of the nanopores and chemical composition of the AAO walls are controlled by the operating conditions during the anodization process. Hence, luminescent properties of AAO can be steered by the operating conditions.

10. Anodization of aluminum alloys

Anodic alumina is also being formed on technical purity aluminum, containing various alloying elements and on the aluminum alloys. Anodization of technical purity aluminum provides poor arrangement of the nanopores due to the substrate chemical inhomogeneities [306]. Nevertheless, various approaches are being undertaken to conduct successful anodization of aluminum-containing alloys.

Zhou et al. [307] reported anodization of zinc-containing aluminum alloy. Three main various anodic layers have been distinguished. The upper layer was made of pure alumina, middle one was made of alumina with incorporated zinc ions, and the bottom layer was made of unoxidized zinc nanopillars.

Additionally, Kondo et al. [308] reported anodization of purple gold, AuAl2 intermetallic alloy. After anodic alumina removal, there were hexagonally arranged hemispherical gold nanodots with diameter of about 30 nm.

11. Macroscopic effects

AAO pores on convex surfaces attempt to achieve minimal energy by two types of processes. Pore merging occurs, reducing the pore densities and hence volume expansion associated with the AAO growth. Alternately, pore branching occurs, reducing radially inward growth rates since the pores now grow in an angled direction. When adjacent growth fronts meet, they create weakened interfaces which ultimately are regions from which cracks nucleate and propagate. Cracks release built-up stresses. In our experiments, wend that the AAO films are crack free for up to 10 mm thickness for all anodization voltages. This thickness therefore, provides an upper limit for creating viable AAO structures on curved surfaces of 100 mm diameter Al wires. Once the cracks originate, independent 'sectors' of growth are formed. A gradual planarization of the curved AAO fronts is observed and for long anodization, fully planar growth fronts of ordered nanopores are observed. Planarization of the growth front is also an effective way to reduce volume expansion as the number of pores per unit area is reduced and this reduces volume expansion and associated stresses [309].

12. Conclusion and future challenges and perspectives

1. The formation of a porous alumina layer starts and expands from the state of the barrier layer formed on the Al surface at the start of anodization. The barrier oxide layer spreads uniformly throughout the surface, with a consistent distribution of current controlled by a continuing field [190–193]. However, the non-uniform distribution of current within the protruding areas of the aluminum substrate ends up in a rise within the field dissolution of the oxide layer and therefore the local thickening of the porous layer, thus beginning the method of cavity formation. During the formation of the oxide layer within the steady state, therefore migration of $Al^{3+}$and OH^{-} and O^{-2} ions in opposite directions, and a part of the Al^{3+}ions, which are driven directly into the electrolyte solution, haven't any role within the formation of the oxide layer.

2. OH-and O^{-2} ions are the foremost important factors within the formation of the porous oxide layer, each of which enters the anodization through its own reactions. These ions that penetrate the plasma membrane define the properties of the porous alumina layer. Binary and tertiary structures are proposed for the membrane; in both cases the inner layer of the wall consists of pure alumina. Within the structure of porous alumina, empty spaces are observed on the ideas of the protrusions of the aluminum substrate, on the joint surface of the metal and therefore the oxide, within the inner layer of the cell walls, which are created to face up to the pressure within the layer. Given the above, geometric parameters like the pore diameter, the gap between the cavities and therefore the wall thickness of the cells may be controlled by factors like anodization voltage, electrolyte temperature, electrolyte concentration and other factors.

Authors' contributions

Ahmed Mahdi Rheima, Zainab sabri Abbas, Mustafa M. Kadhim, Srwa Hashim Mohammed: reviewing and editing.

Dheyaa Yahaia Alhameedi, Fadhil A. Rasen, Alaa dhari jawad al-bayati, Montather F. Ramadan, Zainab Talib Abed, Asala Salam Jaber, Safa K. Hachim, Farah K. Ali, Zaid H Mahmoud: reviewing and editing.

Ehsan Kianfar: Investigation, writing – original draft, reviewing and editing.

Consent for publication

Not applicable.

Funding

Not applicable.

Declaration of competing interest

The authors declare that they have no known competing financial interests or personal relationships that could have appeared to influence the work reported in this paper.

Data availability

The data that has been used is confidential.

Acknowledgment

Mechanical Engineering Department, Faculty of Engineering and Pure Sciences Istanbul Medeniyet University, Istanbul, Turkey.

Young Researchers and Elite Club, Gachsaran Branch, Islamic Azad University, Gachsaran, Iran.

Department of Chemical Engineering, Arak Branch, Islamic Azad University, Arak, Iran.

References

[1] Grzegorz D. Sulka, Leszek Zaraska, Wojciech J. Stepniowski, Anodic porous alumina as a template for nanofabrication, Encyclopedia of nanoscience and nanotechnology 11 (349) (2011) 261–349. Valencia: American Scientific Publishers.

[2] M. Kokonou, A.G. Nassiopoulou, K.P. Giannakopoulos, A. Travlos, T. Stoica, S. Kennou, Growth and characterization of high density stoichiometric SiO_2 dot arrays on Si through an anodic porous alumina template, Nanotechnology 17 (2006) 2146, https://doi.org/10.1088/0957-4484/17/9/011.

[3] G. Patermarakis, K. Moussoutzanis, N. Nikolopoulos, Investigation of the incorporation of electrolyte anions in porous anodic Al_2O_3 films by employing a suitable probe catalytic reaction, J. Solid State Electrochem. 3 (1999) 193–204, https://doi.org/10.1007/s100080050147.

[4] A. Shluger, Defects in oxides in electronic devices, in: W. Andreoni, S. Yip (Eds.), Handbook of Materials Modeling, Springer, Cham, 2019, https://doi.org/10.1007/978-3-319-50257-1_79-1.

[5] R. Abdel-Karim, A. F. Waheed Nanocoatings, Modern Surface Engineering Treatments, Mahmood Aliofkhazraei, IntechOpen, 2013, https://doi.org/10.5772/55776. Available from: https://www.intechopen.com/chapters/44877.

[6] M. Paz Martínez-Viademonte, S.T. Abrahami, T. Hack, M. Burchardt, H. Terryn, A review on anodizing of aerospace aluminum alloys for corrosion protection, Coatings 10 (2020) 1106, https://doi.org/10.3390/coatings10111106.

[7] L. Péter, Preparation of nanoporous oxides from metals by electrochemical anodization, in: Electrochemical Methods of Nanostructure Preparation. Monographs in Electrochemistry, Springer, Cham, 2021, https://doi.org/10.1007/978-3-030-69117-2_13.

[8] http://sundoc.bibliothek.uni-halle.de/diss-online/04/04H055/t2.pdf, 2004 (last accessed 09/2020.

[9] Toshiaki Kondo, Sanami Nagao, Shota Hirano, Takashi Yanagishita, Nhat Truong Nguyen, Patrik Schmuki, Hideki Masuda, Fabrication of ideally ordered anodic porous TiO2 byanodization of pretextured two-layered metals, Electrochem. Commun. 72 (2016) 100–103.

[10] S.Z. Chu, K. Wada, S. Inoue, M. Isogai, Y. Katsuta, A. Yasumori, Large-scale fabrication of ordered nanoporous alumina films with arbitrary pore intervals by critical-potential anodization, J. Electrochem. Soc. 153 (9) (2006) B384–B391.

[11] A. Eftekhari, in: Nanostructured Materials in Electrochemistry, first ed., USA: WILEY-VCH Verlag GmbH & Co. KGaA, Weinheim, 2008.

[12] H. Fzhao, L. Liu, Y. Lei, A mini review: functional nanostructuring with perfectly-ordered anodic aluminum oxide template for energy conversion and storage, Front. Chem. Sci. Eng. 12 (2018) 481–493, https://doi.org/10.1007/s11705-018-1707-x.

[13] B. Yilmaz, B. Yüksel, G. Orhan, D. Aydin, Z. Utlu, Synthesis and characterization of salt-impregnated anodic aluminum oxide composites for low-grade heat storage, Int. J. Miner. Metall. Mater. 27 (2020) 112–118, https://doi.org/10.1007/s12613-019-1890-x.

[14] T. Du, S. Ma, X. Pei, et al., Bio-inspired design and fabrication of micro/nano-brush dual structural surfaces for switchable oil adhesion and antifouling, Small 13 (2017), 1602020, https://doi.org/10.1002/smll.201602020.

[15] S. Ma, M. Scaraggi, P. Lin, B. Yu, D. Wang, D. Dini, F. Zhou, Nanohydrogel brushes for switchable underwater adhesion, J. Phys. Chem. C 121 (2017) 8452–8463, https://doi.org/10.1021/acs.jpcc.7b01305.

[16] R. Zhang, L. Zhang, N. Tian, S. Ma, Y. Liu, B. Yu, X. Pei, F. Zhou, The Tethered fibrillar hydrogels brushes for underwater antifouling, Adv. Mater. Interfac. 4 (2017), https://doi.org/10.1002/admi.201601039.

[17] S. Kim, S. Hyun, J. Lee, K.S. Lee, W. Lee, J.K. Kim, Anodized aluminum oxide/polydimethylsiloxane hybrid mold for roll-to-roll nanoimprinting, Adv. Funct. Mater. 28 (2018), 1800197, https://doi.org/10.1002/adfm.201800197.

[18] W. Xin, Z. Zhang, X. Huang, Y. Hu, T. Zhou, C. Zhu, X.Y. Kong, L. Jiang, L. Wen, High-performance silk-based hybrid membranes employed for osmotic energy

conversion, Nat. Commun. 10 (2019) 3876, https://doi.org/10.1038/s41467-019-11792-8.
[19] M. Amouzadeh Tabrizi, J. Ferré-Borrull, L.F. Marsal, Highly sensitive remote biosensor for the determination of lead (II) ions by using nanoporous anodic alumina modified with DNAzyme, Sensor. Actuator. B Chem. 321 (2020), 128314, https://doi.org/10.1016/j.snb.2020.128314.
[20] Y. Ma, J. Kaczynski, C. Ranacher, A. Roshanghias, M. Zauner, B. Abasahl, Nano-porous aluminum oxide membrane as filtration interface for optical gas sensor packaging, Microelectron. Eng. 198 (2018) 29–34, https://doi.org/10.1016/j.mee.2018.06.013.
[21] W. Chen, X. Gui, B. Liang, R. Yang, Y. Zheng, C. Zhao, X. Li, H. Zhu, Z. Tang, Structural engineering for high sensitivity, ultrathin pressure sensors based on wrinkled graphene and anodic aluminum oxide membrane, ACS Appl. Mater. Interfaces 9 (2017) 24111–24117, https://doi.org/10.1021/acsami.7b05515.
[22] H.O. Ali, Review of porous anodic aluminium oxide (AAO) applications for sensors, MEMS and biomedical devices, Trans. Inst. Met. Finish. 95 (2017) 290–296, https://doi.org/10.1080/00202967.2017.1358514.
[23] J. Chen, S. Wang, L. Ding, Y. Jiang, H. Wang, Performance of through-hole anodic aluminum oxide membrane as a separator for lithium-ion battery, J. Membr. Sci. 461 (2014) 22–27, https://doi.org/10.1016/j.memsci.2014.03.005.
[24] L. Zhou, Y. Tan, D. Ji, B. Zhu, P. Zhang, J. Xu, Q. Gan, Z. Yu, J. Zhu, Self-assembly of highly efficient, broadband plasmonic absorbers for solar steam generation, Sci. Adv. 2 (2016), e1501227, https://doi.org/10.1126/sciadv.1501227.
[25] M.A. Hussain, M. Irshad, E.U. Haq, S. Park, M. Atif, A.S. Hakeem, B.G. Choi, J. W. Kim, Porous anodic aluminum oxide as an efficient support for ruthenium-catalyzed aerobic oxidation of alcohols and amines, Ind. Eng. Chem. Res. 58 (2019) 23025–23031, https://doi.org/10.1021/acs.iecr.9b06054.
[26] Y. Yu, X.-J. Wu, M. Zhao, Q. Ma, J. Chen, B. Chen, M. Sindoro, J. Yang, S. Han, Q. Lu, H. Zhang, Anodized aluminum oxide templated synthesis of metal-organic frameworks used as membrane reactors, Angew. Chem. 129 (2017) 593–596, https://doi.org/10.1002/ange.201610291.
[27] X.F. Zhu, D.D. Li, Y. Song, Y.H. Xiao, The study on oxygen bubbles of anodic alumina based on high purity aluminum, Mater. Lett. 59 (2005) 3160–3163.
[28] K. Shimizu, H. Habazaki, P. Skeldon, Role of metal ion impurities in generation of oxygen gas within anodic alumina, Electrochim. Acta 47 (2002) 1225–1228.
[29] D.I. Petukhov, E.A. Chernova, O.O. Kapitanova, O.V. Boytsova, R.G. Valeev, A. P. Chumakov, O.V. Konovalov, A.A. Eliseev, Thin graphene oxide membranes for gas dehumidification, J. Membr. Sci. 577 (2019) 184–194, https://doi.org/10.1016/j.memsci.2019.01.041.
[30] N.T. Phuong, A. Andisetiawan, D. Van Lam, Nano sand filter with functionalized nanoparticles embedded in anodic aluminum oxide templates, Sci. Rep. 6 (2016) 1–8, https://doi.org/10.1038/srep37673.
[31] K. Liu, Z. Huang, A. Hemmatifar, D.I. Oyarzun, J. Zhou, J.G. Santiago, Self-cleaning porous surfaces for dry condensation, ACS Appl. Mater. Interfaces 10 (2018) 26759–26764, https://doi.org/10.1021/acsami.8b07261.
[32] A. ufani, G. Ozaydin Ince, Protein gating by vapor deposited Janus membranes, J. Membr. Sci. 575 (2019) 126–134, https://doi.org/10.1016/j.memsci.2019.01.013.
[33] D. Wu, D. Zhang, Y. Ye, L. Ma, B. Minhas, B. Liu, H.A. Terryn, J.M.C. Mol, X. Li, Durable lubricant-infused anodic aluminum oxide surfaces with high-aspect-ratio nanochannels, Chem. Eng. J. (Lausanne) 368 (2019) 138–147, https://doi.org/10.1016/j.cej.2019.02.163.
[34] X. Dong, F. Tong, K.M. Hanson, R.O. al-Kaysi, D. Kitagawa, S. Kobatake, C. J. Bardeen, Hybrid Organic-inorganic photon-powered actuators based on aligned diarylethene nanocrystals, Chem. Mater. 31 (2019) 1016–1022, https://doi.org/10.1021/acs.chemmater.8b04568.
[35] N. Chen, D.H. Kim, P. Kovacik, H. Sojoudi, M. Wang, K.K. Gleason, Polymer thin films and surface modification by chemical vapor deposition: recent progress, Annu. Rev. Chem. Biomol. Eng. 7 (2016) 373–393, https://doi.org/10.1146/annurev-chembioeng-080615-033524.
[36] E. Linga Reddy, H.C. Lee, D.H. Kim, Steam reforming of methanol over structured catalysts prepared by electroless deposition of Cu and Zn on anodically oxidized alumina, Int. J. Hydrogen Energy 40 (2015) 2509–2517, https://doi.org/10.1016/j.ijhydene.2014.12.094.
[37] S. Ono, H. Ichinose, N. Masuko, Lattice images of crystalline anodic alumina formed on a ridged aluminum substrate, J. Electrochem. Soc. 139 (1992) 80–81.
[38] A. rzózka, K. Fic, J. Bogusz, A. Brudzisz, M. Marzec, M. Gajewska, G. Sulka, Polypyrrole–nickel hydroxide hybrid nanowires as future materials for energy storage, Nanomaterials 9 (2019) 307, https://doi.org/10.3390/nano9020307.
[39] J. Shang, S. Lin, P. Theato, Fabrication of color changeable CO 2 sensitive nanofibers, Polym. Chem. 8 (2017) 7446–7451, https://doi.org/10.1039/C7PY01628J.
[40] K. Nielsch, J. Choi, K. Schwirn, R.B. Wehrspohn, U. Gösele, Self-Ordering regimes of porous alumina: the 10% porosity rule, Nano Lett. 2 (2002) 677–680.
[41] S.-K. Hwang, S.-H. Jeong, H.-Y. Hwang, O.-J. Lee, K.-H. Lee, Fabrication of highly ordered pore array in anodic aluminum oxide, Kor. J. Chem. Eng. 19 (2002) 467–473.
[42] G.D. Sulka, K.G. Parkola, Temperature influence on well-ordered nanopore structures grown by anodization of aluminium in sulphuric acid, Electrochim. Acta 52 (2007) 1880–1888.
[43] A. Pathak, A. Bora, B. Braunschweig, C. Meltzer, H. Yan, P. Lemmens, W. Daum, J. Schwartz, M. Tornow, Nanocylindrical confinement imparts highest structural order in molecular self-assembly of organophosphonates on aluminum oxide, Nanoscale 9 (2017) 6291–6295, https://doi.org/10.1039/c7nr02420g.
[44] A.M. Mebed, A.M. Abd-Elnaiem, N.M. Al-Hosiny, Electrochemical fabrication of 2D and 3D nickel nanowires using porous anodic alumina templates, Appl. Phys. Mater. Sci. Process 122 (2016) 565, https://doi.org/10.1109/TMAG.2019.2942946.
[45] M. Nehra, A.N. Dilbaghi, V. Singh, N.K. Singhal, S. Kumar, Highly ordered and crystalline Cu nanowires in anodic aluminum oxide membranes for biomedical applications, Phys. Status Solidi A 217 (2020), 1900842, https://doi.org/10.1002/pssa.201900842.
[46] Z.-X. Fang, C.-W. Chu, C.-C. Tsai, C.W. Chang, M.H. Cheng, C.C. Chang, J.T. Chen, Rayleigh-instability-induced transformation for confined polystyrene nanotubes prepared using the solvent-vapor-induced wetting method, Macromol. Mater. Eng. 305 (2020), 1900465, https://doi.org/10.1002/mame.201900465.
[47] K. hat, W. Tu, A. Beena Unni, M. Geppert-Rybczyńska, K. Adrjanowicz, Study on the glass transition dynamics and crystallization kinetics of molecular liquid, dimethyl phthalate, confined in anodized aluminum oxide (AAO) nanopores with atomic layer deposition (ALD) coatings, J. Mol. Liq. 311 (2020), 113296, https://doi.org/10.1016/j.molliq.2020.113296.
[48] K. Lee, H. Kim, J.H. Kim, D. Choi, Structural color and near-infrared tunability of ruthenium-coated anodic aluminum oxide by atomic layer deposition, Scripta Mater. 187 (2020) 125–129, https://doi.org/10.1016/j.scriptamat.2020.06.007.
[49] A. Haider, P. Deminskyi, M. Yilmaz, K. Elmabruk, I. Yilmaz, N. Biyikli, Long-range ordered vertical III-nitride nano-cylinder arrays via plasma-assisted atomic layer deposition, J. Mater. Chem. C 6 (2018) 6471–6482, https://doi.org/10.1039/C8TC01165F.
[50] L. Pol, L.K. Acosta, J. Ferré-Borrull, L.F. Marsal, Aptamer-based nanoporous anodic alumina interferometric biosensor for real-time thrombin detection, Sensors 19 (2019) 4543, https://doi.org/10.3390/s19204543.
[51] C.-T. Liu, Y.-L. Lin, C.-W. Chu, C.W. Chang, Y.J. Chiu, T.Y. Chiu, L.R. Lee, J. T. Chen, Asymmetries in porous membranes: fabrication of anodic aluminum oxide membranes with double-sized nanopores and controlled surface properties, J. Phys. Chem. C 123 (2019) 14540–14546, https://doi.org/10.1021/acs.jpcc.9b03079.
[52] R. Winkler, W. Tu, L. Laskowski, K. Adrjanowicz, Effect of surface chemistry on the glass-transition dynamics of poly(phenyl methyl siloxane) confined in alumina nanopores, Langmuir 36 (2020) 7553–7565, https://doi.org/10.1021/acs.langmuir.0c01194.
[53] J. Wang, S. Pan, Electrodeposition of vertically standing Ag nanoplates and nanowires on transparent conductive electrode using porous anodic aluminum oxide template, Nanotechnology 28 (2017), 425601, https://doi.org/10.1088/1361-6528/aa8614.
[54] L.-R. Lee, V.K. Karapala, Y.-L. Lin, H.C. He, J.T. Chen, Intelligent environmental sensing: fabrication of switchable, reusable, and highly sensitive gas sensors with spiropyran-grafted anodic aluminum oxide templates, J. Phys. Chem. C 124 (2020) 11870–11876, https://doi.org/10.1021/acs.jpcc.0c01129.
[55] E. Wassel, M. Es-Souni, A. Laghrissi, A. Roth, M. Dietze, M. Es-Souni, Data supporting polymerization of anti-fouling polymer brushes polymerized on the pore walls of porous aluminium and titanium oxides, Data Brief 23 (2019), 103702, https://doi.org/10.1016/j.dib.2019.103702.
[56] P. Muanchan, T. Kurose, H. Ito, Replication of mesoscale pore one-dimensional nanostructures: surface-induced phase separation of polystyrene/poly(vinyl alcohol) (PS/PVA) blends, Polymers 11 (2019) 1039, https://doi.org/10.3390/polym11061039.
[57] A. Rath, P. Theato, Advanced AAO templating of nanostructured stimuli-responsive polymers: hype or hope? Adv. Funct. Mater. 30 (2020), 1902959 https://doi.org/10.1002/adfm.201902959.
[58] X. Huang, H. Mutlu, P. Theato, A bioinspired hierarchical underwater superoleophobic surface with reversible pH response, Adv. Mater. Interfac. 7 (2020), 2000101, https://doi.org/10.1002/admi.202000101.
[59] A.P. Leontiev, O.Y. Volkova, I.A. Kolmychek, A.V. Venets, A.R. Pomozov, V. S. Stolyarov, T.V. Murzina, K.S. Napolskii, Tuning the optical properties of hyperbolic metamaterials by controlling the volume fraction of metallic nanorods, Nanomaterials 9 (2019) 739, https://doi.org/10.3390/nano9050739.
[60] M. Salimi, V. Pirouzfar, E. Kianfar, Enhanced gas transport properties in silica nanoparticle filler-polystyrene nanocomposite membranes, Colloid Polym. Sci. 295 (2017) 215–226, https://doi.org/10.1007/s00396-016-3998-0.
[61] E. Kianfar, Synthesis and characterization of AlPO4/ZSM-5 catalyst for methanol conversion to dimethyl ether, Russ. J. Appl. Chem. 91 (2018) 1711–1720, https://doi.org/10.1134/S1070427218100208.
[62] E. Kianfar, Ethylene to propylene conversion over Ni-W/ZSM-5 catalyst, Russ. J. Appl. Chem. 92 (2019) 1094–1101, https://doi.org/10.1134/S1070427219080068.
[63] E. Kianfar, M. Salimi, F. Kianfar, et al., CO2/N2 separation using polyvinyl chloride iso-phthalic acid/aluminium nitrate nanocomposite membrane, Macromol. Res. 27 (2019) 83–89, https://doi.org/10.1007/s13233-019-7009-4.
[64] E. Kianfar, Ethylene to propylene over zeolite ZSM-5: improved catalyst performance by treatment with CuO, Russ. J. Appl. Chem. 92 (2019) 933–939, https://doi.org/10.1134/S1070427219070085.
[65] E. Kianfar, M. Shirshahi, F. Kianfar, et al., Simultaneous prediction of the density, viscosity and electrical conductivity of pyridinium-based hydrophobic ionic liquids using artificial neural network, Silicon 10 (2018) 2617–2625, https://doi.org/10.1007/s12633-018-9798-z.
[66] M. Salimi, V. Pirouzfar, E. Kianfar, Novel nanocomposite membranes prepared with PVC/ABS and silica nanoparticles for C2H6/CH4 separation, Polym. Sci. 59 (2017) 566–574, https://doi.org/10.1134/S0965545X17040071.
[67] F. Kianfar, E. Kianfar, Synthesis of isophthalic acid/aluminum nitrate thin film nanocomposite membrane for hard water softening, J. Inorg. Organomet. Polym. 29 (2019) 2176–2185, https://doi.org/10.1007/s10904-019-01177-1.

[68] E. Kianfar, R. Azimikia, S.M. Faghih, Simple and strong dative attachment of α-diimine nickel (II) catalysts on supports for ethylene polymerization with controlled morphology, Catal. Lett. 150 (2020) 2322–2330, https://doi.org/10.1007/s10562-020-03116-z.
[69] E. Kianfar, Nanozeolites: synthesized, properties, applications, J. Sol. Gel Sci. Technol. 91 (2019) 415–429, https://doi.org/10.1007/s10971-019-05012-4.
[70] H. Liu, E. Kianfar, Investigation the synthesis of nano-SAPO-34 catalyst prepared by different templates for MTO process, Catal. Lett. (2020), https://doi.org/10.1007/s10562-020-03333-6.
[71] E. Kianfar, M. Salimi, S. Hajimirzaee, B. Koohestani, Methanol to gasoline conversion over CuO/ZSM-5 catalyst synthesized using sonochemistry method, Int. J. Chem. React. Eng. 17 (2018).
[72] E. Kianfar, M. Salimi, V. Pirouzfar, B. Koohestani, Synthesis of modified catalyst and stabilization of CuO/NH4-ZSM-5 for conversion of methanol to gasoline, Int. J. Appl. Ceram. Technol. 15 (2018) 734–741, https://doi.org/10.1111/ijac.12830.
[73] Ehsan Kianfar, Mahmoud Salimi, Vahid Pirouzfar, Behnam Koohestani, Synthesis and modification of zeolite ZSM-5 catalyst with solutions of calcium carbonate (CaCO3) and sodium carbonate (Na2CO3) for methanol to gasoline conversion, Int. J. Chem. React. Eng. 16 (7) (2018), 20170229, https://doi.org/10.1515/ijcre-2017-0229.
[74] Ehsan kianfar, Comparison and assessment of Zeolite Catalysts Performance Dimethyl ether and light olefins production through methanol: a review, Rev. Inorg. Chem. 39 (2019) 157–177.
[75] Ehsan Kianfar, Mahmoud Salimi, A review on the production of light olefins from hydrocarbons cracking and methanol conversion, in: James C. Taylor (Ed.), Book: Advances in Chemistry Research, vol. 59, Publisher: Nova Science Publishers, Inc., NY, USA, 2020. Chapter: 1.
[76] Ehsan Kianfar, Razavi Ali, Zeolite catalyst based selective for the process MTG: a review: in book: zeolites, in: Annett Mahler (Ed.), Advances in Research and Applications, Publisher: Nova Science Publishers, Inc., NY, USA, 2020. Chapter: 8.
[77] Ehsan Kianfar, Zeolites: properties, applications, modification and selectivity, in: Annett Mahler (Ed.), Book: Zeolites: Advances in Research and Applications, Publisher: Nova Science Publishers, Inc., NY, USA, 2020. Chapter: 1.
[78] E. Kianfar, S. Hajimirzaee, S.S. Musavian, A.S. Mehr, Zeolite-based catalysts for methanol to gasoline process: a review, Microchem. J. (2020), 104822.
[79] Ehsan Kianfar, Mehdi Baghernejad, Yasaman Rahimdashti, Study synthesis of vanadium oxide nanotubes with two template hexadecylamin and hexylamine, Biological Forum 7 (2015) 1671–1685.
[80] Ehsan kianfar, Synthesizing of Vanadium Oxide Nanotubes Using Hydrothermal and Ultrasonic Method, Publisher: Lambert Academic Publishing, 2020, pp. 1–80, 978-613-9-81541-8.
[81] E. Kianfar, V. Pirouzfar, H. Sakhaeinia, An experimental study on absorption/stripping CO2 using Mono-ethanol amine hollow fiber membrane contactor, J. Taiwan Inst. Chem. Eng. 80 (2017) 954–962.
[82] E. Kianfar, C. Viet, Polymeric membranes on base of PolyMethyl methacrylate for air separation: a review, J. Mater. Res. Technol. 10 (2021) 1437–1461.
[83] S.s. nmousavian, P. Faravar, Z. Zarei, R. zimikia, M.G. Monjezi, E. kianfar, Modeling and simulation absorption of CO2 using hollow fiber membranes (HFM) with mono-ethanol amine with computational fluid dynamics, J. Environ. Chem. Eng. 8 (4) (2020), 103946.
[84] Zhidong Yang, Liehui Zhang, Yuhui Zhou, Hui Wang, Lichen Wen, and Ehsan Kianfar, Investigation of effective parameters on SAPO-34 Nano catalyst the methanol-to-olefin conversion process: a review, Rev. Inorg. Chem. 40 (3) (2020) 91–105, https://doi.org/10.1515/revic-2020-0003.
[85] J. Guo, J. Gao, C. Xiao, L. Chen, L. Qian, Mechanochemical reactions of GaN-Al2O3 interface at the nanoasperity contact: roles of crystallographic polarity and ambient humidity, Friction (2021), https://doi.org/10.1007/s40544-021-0501-9.
[86] Z. Yang, P. Xu, W. Wei, G. Gao, N. Zhou, G. Wu, Influence of the crosswind on the pantograph arcing dynamics, IEEE Trans. Plasma Sci. 48 (8) (2020) 2822–2830, https://doi.org/10.1109/TPS.2020.3010553.
[87] K. Zhang, Q. Wang, L. Chao, J. Ye, Z. Li, Z. Ju Yu, Q. Ground observation-based analysis of soil moisture spatiotemporal variability across a humid to semi-humid transitional zone in China, J. Hydrol. 574 (2019) 903–914, https://doi.org/10.1016/j.jhydrol.2019.04.087.
[88] C.L.L.L. Min Yanga, Predictive model of convective heat transfer coefficient in bone micro-grinding using nanofluid aerosol cooling, Int. Commun. Heat Mass Tran. 125 (105317) (2021), https://doi.org/10.1016/j.icheatmasstransfer.2021.105317.
[89] T. Gao, X. Zhang, C. Li, Y. Zhang, M. Yang, D. Jia, L. Zhu, Surface morphology evaluation of multi-angle 2D ultrasonic vibration integrated with nanofluid minimum quantity lubrication grinding, J. Manuf. Process. 51 (2020) 44–61, https://doi.org/10.1016/j.jmapro.2020.01.024.
[90] Y. Wang, C. Li, Y. Zhang, M. Yang, B. Li, D. Jia, C. Mao, Experimental evaluation of the lubrication properties of the wheel/workpiece interface in minimum quantity lubrication (MQL) grinding using different types of vegetable oils, J. Clean. Prod. 127 (2016) 487–499, https://doi.org/10.1016/j.jclepro.2016.03.121.
[91] Y. Yang, H. Chen, X. Zou, X. Shi, W. Liu, L. Feng, Z. Chen, Flexible carbon-fiber/semimetal Bi nanosheet arrays as separable and recyclable plasmonic photocatalysts and photoelectrocatalysts, ACS Appl. Mater. Interfaces 12 (22) (2020) 24845–24854, https://doi.org/10.1021/acsami.0c05695.
[92] L. Zhang, M. Zhang, S. You, D. Ma, J. Zhao, Z. Chen, Effect of Fe3+ on the sludge properties and microbial community structure in a lab-scale A2O process, Sci. Total Environ. 780 (2021), 146505, https://doi.org/10.1016/j.scitotenv.2021.146505.
[93] H. Chen, A.A. Heidari, H. Chen, M. Wang, Z. Pan, A.H. Gandomi, Multi-population differential evolution-assisted Harris hawks optimization: framework and case studies, Future Generat. Comput. Syst. 111 (2020) 175–198, https://doi.org/10.1016/j.future.2020.04.008.
[94] M. Wang, H. Chen, Chaotic multi-swarm whale optimizer boosted support vector machine for medical diagnosis, Appl. Soft Comput. 88 (2020), 105946, https://doi.org/10.1016/j.asoc.2019.105946.
[95] a Y. Xu, H. Chen, J. Luo, Q. Zhang, S. Jiao, X. Zhang, Enhanced Moth-flame optimizer with mutation strategy for global optimization, Inf. Sci. 492 (2019) 181–203, https://doi.org/10.1016/j.ins.2019.04.022;
b X. Zhao, X. Zhang, Z. Cai, X. Tian, X. Wang, Y. Huang, H. Chen, L. Hu, Chaos enhanced grey wolf optimization wrapped ELM for diagnosis of paraquat-poisoned patients, Comput. Biol. Chem. (2019) 481–490, https://doi.org/10.1016/j.compbiolchem.2018.11.017.
[96] C. Li, L. Hou, B. Sharma, H. Li, C. Chen, Y. Li, X. Zhao, H. Huang, Z. Cai, H. Chen, Developing a new intelligent system for the diagnosis of tuberculous pleural effusion, Comput. Methods Progr. Biomed. 153 (2018) 211–225, https://doi.org/10.1016/j.cmpb.2017.10.022.
[97] M. Wang, H. Chen, B. Yang, X. Zhao, L. Hu, Z. Cai, H. Huang, C. Tong, Toward an optimal kernel extreme learning machine using a chaotic moth-flame optimization strategy with applications in medicaldiagnoses, Neurocomputing 267 (2017) 6984, https://doi.org/10.1016/j.neucom.2017.04.060.
[98] J. Xia, H. Chen, Q. Li, M. Zhou, L. Chen, Z. Cai, Y. Fang, H. Zhou, Ultrasound-based differentiation of malignant and benign thyroid Nodules: an extreme learning machine approach, Comput. Methods Progr. Biomed. 147 (2017) 37–49, https://doi.org/10.1016/j.cmpb.2017.06.005.
[99] H.-L. Chen, G. Wang, C. Ma, Z.-N. Cai, W.-B. Liu, S.-J. Wang, An efficient hybrid kernel extreme learning machine approach for early diagnosis of Parkinson's disease, Neurocomputing 184 (2016) 131–144, https://doi.org/10.1016/j.neucom.2015.07.138.
[100] L. Shen, H. Chen, Z. Yu, W. Kang, B. Zhang, H. Li, B. Yang, D. Liu, Evolving support vector machines using fruit fly optimization for medical data classification, Knowl. Base Syst. 96 (2016) 61–75, https://doi.org/10.1016/j.knosys.2016.01.002.
[101] Lufeng Hu, G. Hong, Jianshe Ma, Xianqin Wang, Huiling Chen, An efficient machine learning approach for diagnosis of paraquat-poisoned patients, Comput. Biol. Med. 59 (2015) 116–124, https://doi.org/10.1016/j.compbiomed.2015.02.003.
[102] X. Xu, H.-L. Chen, Adaptive computational chemotaxis based on field in bacterial foraging optimization, Soft Comput. 18 (4) (2014) 797–807, https://doi.org/10.1007/s00500-013-1089-4.
[103] Chengyun Gao, Jiayou Liao, Jingqiong Lu, Jiwei Ma, Ehsan Kianfar, The effect of nanoparticles on gas permeability with polyimide membranes and network hybrid membranes: a review, Rev. Inorg. Chem. (2020), https://doi.org/10.1515/revic-2020-0007.
[104] Ehsan Kianfar, Mahmoud Salimi, Behnam Koohestani, Zeolite CATALYST: A Review on the Production of Light Olefins, Publisher: Lambert Academic Publishing, 2020, pp. 1–116, 978-620-3-04259-7.
[[105]] .
[106] .
[107] .
[108] Ehsan Kianfar, Investigation on Catalysts of "Methanol to Light Olefins", Publisher: Lambert Academic Publishing, 2020, pp. 1–168, 978-620-3-19402-9.
[109] E. Kianfar, Application of Nanotechnology in Enhanced Recovery Oil and Gas Importance & Applications of Nanotechnology, vol. 5, MedDocs Publishers, 2020, pp. 16–21 (Chapter 3).
[110] E. Kianfar, Catalytic Properties of Nanomaterials and Factors Affecting it . Importance & Applications of Nanotechnology, vol. 5, MedDocs Publishers, 2020, pp. 22–25 (Chapter 4).
[111] E. Kianfar, Introducing the Application of Nanotechnology in Lithium-Ion Battery Importance & Applications of Nanotechnology, vol. 4, MedDocs Publishers, 2020, pp. 1–7 (Chapter 4).
[112] Ehsan Kianfar, H. Mazaheri, Synthesis of nanocomposite (CAU-10-H) thin-film nanocomposite (TFN) membrane for removal of color from the water, Fine Chemical Engineering 1 (2020) 83–91.
[113] Ehsan Kianfar, Mahmoud Salimi, Behnam Koohestani, Methanol to gasoline conversion over CuO/ZSM-5 catalyst synthesized and influence of water on conversion, Fine Chemical Engineering 1 (2020) 75–82.
[114] Ehsan Kianfar, An experimental study PVDF and PSF hollow fiber membranes for chemical absorption carbon dioxide, Fine Chemical Engineering 1 (2020) 92–103.
[115] Ehsan Kianfar, Sajjad Mafi, Ionic liquids: properties, application, and synthesis, Fine Chemical Engineering 2 (2020) 22–31.
[116] S.M. Faghih, E. Kianfar, Modeling of fluid bed reactor of ethylene dichloride production in Abadan Petrochemical based on three-phase hydrodynamic model, Int. J. Chem. React. Eng. 16 (2018) 1–14.
[117] Ehsan Kianfar, H. Mazaheri, Methanol to gasoline: a sustainable transport fuel, in: Book: Advances in Chemistry Research. James C.taylorChapter: 4Publisher vol. 66, Nova Science Publishers, Inc., NY, USA, 2020.
[118] L. Zhang, J. Zheng, S. Tian, H. Zhang, X. Guan, S. Zhu, Z. Li, Effects of Al3+ on the microstructure and bioflocculation of anoxic sludge, J. Environ. Sci. 91 (2020) 212–221, https://doi.org/10.1016/j.jes.2020.02.01.
[119] X. Cao, Z. Huang, C. He, W. Wu, L. Xi, Y. Li, D. Fang, In-situ synchrotron X-ray tomography investigation of the imperfect smooth-shell cylinder structure,

Compos. Struct. 267 (2021), 113926, https://doi.org/10.1016/j.compstruct.2021.113926.
[120] N. Zhao, L. Deng, D. Luo, P. Zhang, One-step fabrication of biomass-derived hierarchically porous carbon/MnO nanosheets composites for symmetric hybrid supercapacitor, Appl. Surf. Sci. 526 (2020), 146696, https://doi.org/10.1016/j.apsusc.2020.146696.
[121] P. Dong, T. Zhang, H. Xiang, X. Xu, Y. Lv, Y. Wang, C. Lu, Controllable synthesis of exceptionally small-sized superparamagnetic magnetite nanoparticles for ultrasensitive MR imaging and angiography, J. Mater. Chem. B 9 (4) (2021) 958–968, https://doi.org/10.1039/D0TB02337J.
[122] Z. Wang, T. Zhang, L. Pi, H. Xiang, P. Dong, C. Lu, T. Jin, Large-scale one-pot synthesis of water-soluble and biocompatible upconversion nanoparticles for dual-modal imaging, Colloids Surf. B Biointerfaces 198 (2021), 111480, https://doi.org/10.1016/j.colsurfb.2020.111480.
[123] Z. Ni, X. Cao, X. Wang, S. Zhou, C. Zhang, B. Xu, Y. Ni, Facile synthesis of copper (I) oxide nanochains and the photo-thermal conversion performance of its nanofluids, Coatings 11 (2021) 749, https://doi.org/10.3390/coatings11070749.
[124] L. Chen, J. Xu, M. Zhang, T. Rong, Z. Jiang, P. Li, Systematic study on mechanical and electronic properties of ternary VAlN, TiAlN and WAlN systems by first-principles calculations, Ceram. Int. 47 (6) (2021) 7511–7520, https://doi.org/10.1016/j.ceramint.2020.11.090.
[125] Yanbin Zhang, Li Hao Nan, Li Changhe, Chuanzhen Huang, Ali Hafiz Muhammad, Xu Xuefeng, Mao Cong, Ding Wenfeng, Cui Xin, Yang Min, Yu Tianbiao, Jamil Muhammad, Munish Kumar Gupta, Dongzhou Jia, Said Zafar, Nano-enhanced biolubricant in sustainable manufacturing: from processability to mechanisms, Friction (2021), https://doi.org/10.1007/s40544-021-0536-y. In Press.
[126] A. Kianfar, Comparison and assessment on performance of zeolite catalyst based selective for theProcess methanol to gasoline: a review, in: Advances in Chemistry Research, Nova Science Publishers, Inc., NewYork, 2020, p. 63 (Chapter 2).
[127] E. Kianfar, M. Salimi, F. Kianfar, et al., CO2/N2 separation using polyvinyl chloride iso-phthalic acid/aluminium nitrate nanocomposite membrane, Macromol. Res. 27 (2019) 83–89, https://doi.org/10.1007/s13233-019-7009-4.
[128] Ehsan Kianfar, Synthesis of characterization Nanoparticles isophthalic acid/aluminum nitrate (CAU-10-H) using method hydrothermal, Advances in Chemistry Research (2020). NY, USA: Nova Science Publishers, Inc.
[129] Ehsan Kianfar, CO2 capture with ionic liquids: a review, in: Advances in Chemistry Research, vol. 67, Publisher: Nova Science Publishers, Inc., NY, USA, 2020.
[130] Ehsan Kianfar, Enhanced light olefins production via methanol dehydration over promoted SAPO-34, in: Advances in Chemistry Research, vol. 63, Nova Science Publishers, Inc., NY, USA, 2020. Chapter: 4.
[131] Ehsan Kianfar, Gas hydrate: applications, structure, formation, separation processes, Thermodynamics, in: James C. Taylor (Ed.), Advances in Chemistry Research, vol. 62, Publisher: Nova Science Publishers, Inc., NY, USA, 2020. Chapter: 8.
[132] Mehran Kianfar, Farshid Kianfar, Ehsan Kianfar, The effect of nano-composites on the mechanic and morphological characteristics of NBR/PA6 blends, Am. J. Oil Chem. Technol. 4 (1) (2016) 29–44.
[133] Farshad Kianfar, Seyed Reza Mahdavi Moghadam, Ehsan Kianfar, Energy optimization of ilam gas refinery unit 100 by using HYSYS refinery software (2015), Indian Journal of Science and Technology 8 (S9) (2015) 431–436.
[134] Ehsan Kianfar, Production and identification of vanadium oxide nanotubes, Indian Journal of Science and Technology 8 (S9) (2015) 455–464.
[135] Farshad Kianfar, Seyed Reza Mahdavi Moghadam, Ehsan Kianfar, Synthesis of spiro pyran by using silica-bonded N-propyldiethylenetriamine as recyclable basic catalyst, Indian Journal of Science and Technology 8 (11) (2015), 68669.
[136] E. Kianfar, Recent advances in synthesis, properties, and applications of vanadium oxide nanotube, Microchem. J. 145 (2019) 966–978.
[137] Saeed Hajimirzaee, Amin Soleimani Mehr, Ehsan Kianfar, Modified ZSM-5 Zeolite for Conversion of LPG to Aromatics, Polycyclic Aromatic Compounds, 2020, https://doi.org/10.1080/10406638.2020.1833048.
[138] E. Kianfar, Investigation of the effect of crystallization temperature and time in synthesis of SAPO-34 catalyst for the production of light olefins, Petrol. Chem. 61 (2021) 527–537, https://doi.org/10.1134/S0965544121050030.
[139] Xiaoping Huang, Yufang Zhu, Ehsan Kianfar, Nano biosensors: properties, applications and electrochemical techniques, J. Mater. Res. Technol. 12 (2021) 1649–1672, https://doi.org/10.1016/j.jmrt.2021.03.048.
[140] E. Kianfar, Protein nanoparticles in drug delivery: animal protein, plant proteins and protein cages, albumin nanoparticles, J. Nanobiotechnol. 19 (2021) 159, https://doi.org/10.1186/s12951-021-00896-3.
[141] E. Kianfar, Magnetic nanoparticles in targeted drug delivery: a review, J. Supercond. Nov. Magnetism (2021), https://doi.org/10.1007/s10948-021-05932-9.
[142] .
[143] Rahmad Syah, Marziah Zahar, Ehsan Kianfar, Nanoreactors: properties, applications and characterization, Int. J. Chem. React. Eng. (2021), 000010151520210069, https://doi.org/10.1515/ijcre-2021-0069.
[144] H. Thacker, V. Ram, P. Dave, Plant mediated synthesis of Iron nanoparticles and their Applications: a Review, Progress in Chemical and Biochemical Research 2 (3) (2019) 84–91, https://doi.org/10.33945/SAMI/pcbr.2019.183239.1033.
[145] M. Rigi, Antimicrobial activities of gold and silver nanoparticles against Vibrio cholera, International Journal of Advanced Biological and Biomedical Research 4 (1) (2016) 104–107, https://doi.org/10.26655/ijabbr.2016.2.14.
[146] A. Talavari, B. Ghanavati, A. Azimi, S. Sayyahi, PVDF/MWCNT hollow fiber mixed matrix membranes for gas absorption by Al2O3 nanofluid, Progress in Chemical and Biochemical Research 4 (2) (2021) 177–190, https://doi.org/10.22034/pcbr.2021.270178.1177.
[147] S. Ghotekar, H. Dabhane, S. Pansambal, R. Oza, P. Tambade, V. Medhane, A review on biomimetic synthesis of Ag2O nanoparticles using plant extract, characterization and its recent applications, Advanced Journal of Chemistry-Section B 2 (3) (2020) 102–111, https://doi.org/10.22034/ajcb.2020.107810.
[148] M. Fatih Gözükızıl, pH EFFECT ON STRUCTURAL, MORPHOLOGICAL AND OPTICAL PROPERTIES OF ZnO THIN FILMS PRODUCED BY CHEMICAL BATH DEPOSITION METHOD, EUROPEAN CHEMICAL BULLETIN 9 (10) (2020) 335–338.
[149] M. Rakebizadeh, M. Zahedizadeh, Y.E. Panah, Supplemental effect of zinc oxide nanoparticles and mentha spicata butanol extract on blood glucose of diabetic wistar rats, Journal of Research in Science, Engineering and Technology 6 (3) (2018) 1–5.
[150] H. Guan, S. Huang, J. Ding, F. Tian, Q. Xu, J. Zhao, Chemical environment and magnetic moment effects on point defect formations in CoCrNi-based concentrated solid-solution alloys, Acta Mater. 187 (2020) 122–134, https://doi.org/10.1016/j.actamat.2020.01.044.
[151] X. Zhang, Y. Tang, F. Zhang, C. Lee, A novel aluminum-graphite dual-ion battery, Adv. Energy Mater. 6 (11) (2016), 1502588, https://doi.org/10.1002/aenm.201502588.
[152] X. Tong, F. Zhang, B. Ji, M. Sheng, Y. Tang, Carbon-Coated porous aluminum foil anode for high-rate, long-term cycling stability, and high energy density dual-ion batteries, Adv. Mater. 28 (45) (2016) 9979–9985, https://doi.org/10.1002/adma.201603735.
[153] H. Zhu, R. Zhao, Isolated Ni atoms induced edge stabilities and equilibrium shapes of CVD-prepared hexagonal boron nitride on Ni(111) surface, New J. Chem. (2022), https://doi.org/10.1039/D2NJ03735A.
[154] X. Peng, S. Mo, R. Li, J. Li, C. Tian, W. Liu, Y. Wang, Effective removal of the rare earth element dysprosium from wastewater with polyurethane sponge-supported graphene oxide–titanium phosphate, Environ. Chem. Lett. 19 (1) (2021) 719–728, https://doi.org/10.1007/s10311-020-01073-y.
[155] Y. Wu, Y. Zhao, X. Han, G. Jiang, J. Shi, P. Liu, Y. Yamada, Ultra-fast growth of cuprate superconducting films: dual-phase liquid assisted epitaxy and strong flux pinning, Materials Today Physics 18 (2021), 100400, https://doi.org/10.1016/j.mtphys.2021.100400.
[156] Z. Wang, L. Dai, J. Yao, T. Guo, D. Hrynsphan, S. Tatsiana, J. Chen, Improvement of Alcaligenes sp.TB performance by Fe-Pd/multi-walled carbon nanotubes: enriched denitrification pathways and accelerated electron transport, Bioresour. Technol. 327 (2021), 124785, https://doi.org/10.1016/j.biortech.2021.124785.
[157] X. Li, J. Yan, T. Yu, B. Zhang, Versatile nonfluorinated superhydrophobic coating with self-cleaning, anti-fouling, anti-corrosion and mechanical stability, Colloids Surf., A (2022) 642, https://doi.org/10.1016/j.colsurfa.2022.128701.
[158] X. Li, Y. Song, C. Zhang, C. Zhao, C. He, Inverse CO2/C2H2 separation in a pillared-layer framework featuring a chlorine-modified channel by quadrupole-moment sieving, Separ. Purif. Technol. 279 (2021), 119608, https://doi.org/10.1016/j.seppur.2021.119608.
[159] R. Zhang, W. Zhang, Q. Yang, J. Dong, L. Ma, Z. Jiang, Y. Huang, 3D hierarchical oxygen-deficient AlCoNi-(oxy)hydroxides/N–doped carbon hybrids enable efficient battery-type asymmetric supercapacitor, J. Energy Chem. (2022), https://doi.org/10.1016/j.jechem.2022.04.050.
[160] T. Zolfaghari, Synthesis and characterization of a new PAI/ZnO derived from 3, 3-bis (4-(4-aminophenoxy) phenyl) "-2-benzofuran-1-one, J. Synth. Chem. 1 (2022) 52–61, https://doi.org/10.22034/jsc.2022.155231.
[161] M. Ghasemvand, B. Behjat, S. Ebrahimi, Experimental investigation of the effects of adhesive defects on the strength and creep behavior of single-lap adhesive joints at various temperatures, J. Adhes. (2022) 1–17.
[162] M. Shojaie, One-pot Multicomponent synthesis of pyrano[2,3-c]pyrazoles catalyzed by Copper oxide nanoparticles (CuO NPs), J. Synth. Chem. 1 (2022) 125–131, https://doi.org/10.22034/jsc.2022.155286.
[163] H.B. Baniya, R.P. Guragain, D.P. Subedi, Cold atmospheric pressure plasma technology for modifying polymers to enhance adhesion: a critical review, REVIEWS OF ADHESION AND ADHESIVES 9 (2) (2021) 269–307.
[164] P. Brown, P. Mazumder, Current progress in mechanically durable water-repellent surfaces: a critical review, REVIEWS OF ADHESION AND ADHESIVES 9 (1) (2021) 123–152.
[165] J. Müssig, N. Graupner, Test methods for fibre/matrix adhesion in cellulose fibre-reinforced thermoplastic composite materials: a critical review, Rev. Adhesion Adhesives 8 (No. 2) (2021) 68–129.
[166] M.K. Apalak, K. Gul, Y.E. Arslan, Buckling and post-buckling behaviours of adhesively bonded aluminium beams: a review, REVIEWS OF ADHESION AND ADHESIVES 10 (1) (2022) 1–46.
[167] H.B. Desai, A. Kumar, A.R. Tanna, STRUCTURAL AND MAGNETIC PROPERTIES OF MgFe2O4 FERRITE NANOPARTICLES SYNTHESIS THROUGH AUTO COMBUSTION TECHNIQUE, European Chemical Bulletin 10 (3) (2021) 186–190.
[168] A.K. Netam, V.P. Bhargava, R. Singh, P. Sharma, Physico-chemical characterization of ayurvedic swarna bhasma by using SEM, EDAX, XRD and PSA, Journal of Complementary Medicine Research 12 (2) (2021) 204–209, https://doi.org/10.5455/jcmr.2021.12.02.23.
[169] S.D. Wani, A. mundada, A review: emerging trends in bionanocomposites, International Journal of Pharmacy Research & Technology 11 (1) (2021) 1–8, https://doi.org/10.31838/ijprt/11.01.01.
[170] A. Athab, A.J. Lafta, F.H. Hussein, Modification of carbon nanotubes surface using different oxidizing agents, J. Environ. Anal. Chem 2 (2015) e112.
[171] Y.F. Al-Khafaji, M.R. Al-Lami, A.S. Abbas, A.M.E.E.R. Al-Ameri, A.F.A. Mousa, Synthesis and characterization of niobium and tantalum complexes with

bidentate ligand and its use in ring opening polymerization of ε-caprolactone, Asian J. Chem. 30 (2) (2018) 460–462.
[172] M. Yang, C. Li, Y. Zhang, D. Jia, X. Zhang, Y. Hou, R. Li, J. Wang, Maximum undeformed equivalent chip thickness for ductile-brittle transition of zirconia ceramics under different lubrication conditions, Int. J. Mach. Tool Manufact. 122 (2017) 55–65, https://doi.org/10.1016/j.ijmachtools.2017.06.003.
[173] Yanbin Zhang, Li Hao Nan, Li Changhe, Chuanzhen Huang, Ali Hafiz Muhammad, Xu Xuefeng, Mao Cong, Ding Wenfeng, Cui Xin, Yang Min, Yu Tianbiao, Jamil Muhammad, Munish Kumar Gupta, Dongzhou Jia, Said Zafar, Nano-enhanced biolubricant in sustainable manufacturing: from processability to mechanisms, Friction (2021), https://doi.org/10.1007/s40544-021-0536-y.
[174] X. Cui, C.H. Li, W.F. Ding, Y. Chen, C. Mao, X.F. Xu, B. Liu, D.Z. Wang, H.N. Li, Y. B. Zhang, Z. Said, S. Debnath, M. Jamil, H. Muhammad Ali, S. Sharma, Minimum quantity lubrication machining of aeronautical materials using carbon group nanolubricant: from mechanisms to application, Chin. J. Aeronaut. (2021), https://doi.org/10.1016/j.cja.2021.08.011.
[175] Mingzheng Liu, Changhe Li, Yanbin Zhang, Qinglong An, Min Yang, Teng Gao, Cong Mao, Bo Liu, Huajun Cao, Xuefeng Xu, Zafar Said, Sujan Debnath, Muhammad Jamil, Hafz Muhammad Ali, Shubham Sharma, Cryogenic minimum quantity lubrication machining: from mechanism to application, Front. Mech. Eng. 16 (4) (2021) 649–697, https://doi.org/10.1007/s11465-021-0654-2.
[176] Teng Gao, Changhe Li, Yiqi Wang, Xueshu Liu, Qinglong An, Hao Nan Li, Yanbin Zhang, Huajun Cao, Bo Liu, Dazhong Wang, Zafar Said, Sujan Debnath, Muhammad Jamil, Hafiz Muhammad Ali, Shubham Sharma, Carbon fiber reinforced polymer in drilling: from damage mechanisms to suppression, Compos. Struct. 286 (2022), 115232, https://doi.org/10.1016/j.compstruct.2022.115232.
[177] Dongzhou Jia, Yanbin Zhang, Li Changhe, Yang Min, Teng Gao, Zafar Said, Shubham Sharma, Lubrication-enhanced mechanisms of titanium alloy grinding using lecithin biolubricant, Tribol. Int. 169 (2022), 107461, https://doi.org/10.1016/j.triboint.2022.107461.
[178] H.S. Majdi, Z.A. Latipov, V. Borisov, et al., Nano and battery anode: a review, Nanoscale Res. Lett. 16 (2021) 177, https://doi.org/10.1186/s11671-021-03631-x.
[179] Dmitry Bokov, Abduladheem Turki Jalil, Supat Chupradit, Wanich Suksatan, Mohammad Javed Ansari, Iman H. Shewael, Gabdrakhman H. Valiev, Ehsan Kianfar, Nanomaterial by sol-gel method: synthesis and application, Adv. Mater. Sci. Eng. 2021 (2021) 21, https://doi.org/10.1155/2021/5102014. Article ID 5102014.
[180] Supat Chupradit, M. Kavitha, Wanich Suksatan, Mohammad Javed Ansari, I. Zuhair, Mashhadani Al, Mustafa M. Kadhim, Yasser Fakri Mustafa, Shafik S. Shafik, Ehsan Kianfar, Morphological control: properties and applications of metal nanostructures, Adv. Mater. Sci. Eng. 2022 (2022) 15, https://doi.org/10.1155/2022/1971891. Article ID 1971891.
[181] Omer Dhia Aldeen Salah Aldeen, Mustafa Z. Mahmoud, Hasan Sh Majdi, Dhameer A. Mutlak, Khusniddin Fakhriddinovich Uktamov, Ehsan kianfar, Investigation of effective parameters Ce and Zr in the synthesis of H-ZSM-5 and SAPO-34 on the production of light olefins from naphtha, Adv. Mater. Sci. Eng. 2022 (2022), 6165180, https://doi.org/10.1155/2022/6165180, 22 pages.
[182] Asep Suryatna, Indah Raya, Lakshmi Thangavelu, Firas Rahi Alhachami, Mustafa M. Kadhim, Usama S. Altimari, Zaid H. Mahmoud, Yasser Fakri Mustafa, Ehsan Kianfar, A review of high-energy density lithium-air battery technology: investigating the effect of oxides and nanocatalysts, J. Chem. 2022 (2022) 32, https://doi.org/10.1155/2022/2762647. Article ID 2762647.
[183] W.K. Abdelbasset, S.A. Jasim, D.O. Bokov, et al., Comparison and evaluation of the performance of graphene-based biosensors, Carbon Lett 32 (2022) 927–951, https://doi.org/10.1007/s42823-022-00338-6.
[184] S.A. Jasim, M.M. Kadhim, V. Kn, et al., Molecular junctions: introduction and physical foundations, nanoelectrical conductivity and electronic structure and charge transfer in organic molecular junctions, Braz. J. Phys. 52 (2022) 31, https://doi.org/10.1007/s13538-021-01033-z.
[185] E. kianfar, B. Abed Hussein, A. Mahdi, S. Emad Izzat, N. Acwin Dwijendra, R. Romero Parra, L. Barboza Arenas, Y. Mustafa, G. Yasin, A. Thaeer Hammid, Production, Structural properties Nano biochar and Effects Nano biochar in soil: a review, Egypt. J. Chem. 65 (12) (2022), https://doi.org/10.21608/ejchem.2022.131162.5772.
[186] E. kianfar, S. Jasim, H. Kzar, R. Sivaraman, M. Zaidi, O. Alkadir, F. Safaa Fahim, M. Jweeg, A. Obaid Aldulaim, Engineered nanomaterials, plants, plant toxicity and biotransformation: a review, Egypt. J. Chem. 65 (12) (2022), https://doi.org/10.21608/ejchem.2022.131166.5775.
[187] M.J. Ansari, M.M. Kadhim, B.A. Hussein, et al., Synthesis and stability of magnetic nanoparticles, BioNanoSci 12 (2022) 627–638, https://doi.org/10.1007/s12668-022-00947-5.
[188] K. Hachem, M.J. Ansari, R.O. Saleh, et al., Methods of chemical synthesis in the synthesis of nanomaterial and nanoparticles by the chemical deposition method: a review, BioNanoSci 12 (2022) 1032–1057, https://doi.org/10.1007/s12668-022-00996-w.
[189] G.F. Smaisim, D.B. mohammed, A.M. Abdulhadi, et al., Nanofluids: properties and applications, J. Sol. Gel Sci. Technol. 104 (2022) 1–35, https://doi.org/10.1007/s10971-022-05859-0.
[190] E. Kianfar, The effects of SiO2/Al2O3 and H2O/Al2O3 molar ratios on SAPO-34 catalyst in the methanol to olefin process, Silicon (2022), https://doi.org/10.1007/s12633-022-02008-8.
[191] O.D. Salahdin, H. Sayadi, R. Solanki, et al., Graphene and carbon structures and nanomaterials for energy storage, Appl. Phys. A 128 (2022) 703, https://doi.org/10.1007/s00339-022-05789-2.
[192] N.D. Trung, D.T.N. Huy, M. Jade Catalan Opulencia, et al., Conductive gels: properties and applications of nanoelectronics, Nanoscale Res. Lett. 17 (2022) 50, https://doi.org/10.1186/s11671-022-03687-3.
[193] Lawal Adedoyin Isola, Tzu-Chia Chen, Marischa Elveny, Ayad F. Alkaim, Lakshmi Thangavelu, Ehsan Kianfar, Application of micro and porous materials as nano-reactors, Rev. Inorg. Chem. 42 (2) (2022) 121–136, https://doi.org/10.1515/revic-2021-0007.
[194] G.R.L. Al-Awsi, A.A. Alameri, A.M.B. Al-Dhalimy, G.A. Gabr, E. Kianfar, Application of nano-antibiotics in the diagnosis and treatment of infectious diseases, Braz. J. Biol. 84 (2023).
[195] R. Alabada, M.M. Kadhim, Z. sabri Abbas, A.M. Rheima, U.S. Altimari, A. H. Dawood, E. Kianfar, Investigation of Effective Parameters in the Production of Alumina Gel through the Sol-Gel Method, Case Studies in Chemical and Environmental Engineering, 2023, 100405.
[196] L.A. Younus, Z.H. Mahmoud, A.A. Hamza, K.M.A. Alaziz, M.L. Ali, Y. Yasin, E. Kianfar, Photodynamic therapy in cancer treatment: properties and applications in nanoparticles, Braz. J. Biol. 84 (2023), e268892.
[197] G.F. Smaisim, K.J. Mohammed, S.K. Hadrawi, H. Koten, E. Kianfar, Properties and application of nanostructure in liquid crystals, BioNanoScience 13 (2) (2023) 819–839.
[198] K.J. Mohammed, S.K. Hadrawi, E. Kianfar, Synthesis and modification of nanoparticles with ionic liquids: a review, BioNanoScience 13 (2) (2023) 760–783.
[199] Z. sabri Abbas, M.M. Kadhim, A. Mahdi Rheima, A.D. jawad al-bayati, Z. Talib Abed, F.M. dashoor Al-Jaafari, E. Kianfar, Preparing Hybrid Nanocomposites on the Basis of Resole/Graphene/Carbon Fibers for Investigating Mechanical and Thermal Properties, BioNanoScience, 2023, pp. 1–29.
[200] U. Abdul-Reda Hussein, Z.H. Mahmoud, K.M. Abd Alaziz, M.L. Alid, Y. Yasin, F. K. Ali, E. Kianfar, Antimicrobial finishing of textiles using nanomaterials, Braz. J. Biol. 84 (2023), e264947.
[201] Z.H. Mahmoud, H.A. Salman, H.H. Hussein, A.H. Adhab, K. Al-Majdi, T. Rasheed, E. Kianfar, Organic chemical Nano sensors: synthesis, properties, and applications, Braz. J. Biol. 84 (2023), e268893.
[202] M.M. Kadhim, A.M. Rheima, Z.S. Abbas, H.H. Jlood, S.K. Hachim, W.R. Kadhum, Evaluation of a biosensor-based graphene oxide-DNA nanohybrid for lung cancer, RSC Adv. 13 (4) (2023) 2487–2500.
[203] I.M.R. Fattah, Z.A. Farhan, K.J. Kontoleon, E. Kianfar, S.K. Hadrawi, Hollow Fiber Membrane Contactor Based Carbon Dioxide Absorption− Stripping: a Review, Macromolecular Research, 2023, pp. 1–27.
[204] E. Kianfar, The effects of SiO2/Al2O3 and H2O/Al2O3 molar ratios on SAPO-34 catalyst in the methanol to olefin process, Silicon 15 (1) (2023) 381–396.
[205] E. Kianfar, H. Sayadi, Recent advances in properties and applications of nanoporous materials and porous carbons, Carbon Letters (2022) 1–25.
[206] A. Abderrahmane, A. Mourad, S. Mohammed, G.F. Smaisim, D. Toghraie, A. Koulali, O. Younis, Second law analysis of a 3D magnetic buoyancy-driven flow of hybrid nanofluid inside a wavy cubical cavity partially filled with porous layer and non-Newtonian layer, Ann. Nucl. Energy 181 (2023), 109511.
[207] G.F. Smaisim, A.M. Abed, H. Al-Madhhachi, S.K. Hadrawi, H.M.M. Al-Khateeb, E. Kianfar, Graphene-Based Important Carbon Structures and Nanomaterials for Energy Storage Applications as Chemical Capacitors and Supercapacitor Electrodes: a Review, BioNanoScience, 2022, pp. 1–30.
[208] Y. Wang, J. Zheng, G.F. Smaisim, D. Toghraie, Molecular dynamics simulation of phase transition procedure of water-based nanofluid flow containing CuO nanoparticles, Alex. Eng. J. 61 (12) (2022) 12453–12461.
[209] M. Xiao, G.F. Smaisim, Joint chance-constrained multi-objective optimal function of multi-energy microgrid containing energy storages and carbon recycling system, J. Energy Storage 55 (2022), 105842.
[210] A. Mourad, A. Aissa, A.M. Abed, G.F. Smaisim, D. Toghraie, M.A. Fazilati, A. A. Alizadeh, The numerical analysis of the melting process in a modified shell-and-tube phase change material heat storage system, J. Energy Storage 55 (2022), 105827.
[211] G.F. Smaisim, A.M. Abed, H. Alavi, Analysis of pollutant emission reduction in a coal power plant using renewable energy, Int. J. Low Carbon Technol. (2022).
[212] A. Abderrahmane, W. Jamshed, A.M. Abed, G.F. Smaisim, K. Guedri, O.A. Akbari, S. Baghaei, Heat and mass transfer analysis of non-Newtonian power-law nanofluid confined within annulus enclosure using Darcy-Brinkman-Forchheimer model, Case Stud. Therm. Eng. (2022), 102569.
[213] X. Tan, R.F. Obaid, G.F. Smaisim, M.M. Esfahani, F. Alsaikhan, S. Baghaei, A. Yadav, Investigation of addition of calcium phosphate ceramic to multilayer scaffold for bone applications with improved mechanical properties: fuzzy logic analysis, Ceram. Int. (2022).
[214] S. Mir, A.M. Abed, O.A. Akbari, A. Mohammadian, D. Toghraie, A. Marzban, G. F. Smaisim, Effects of curvature existence, adding of nanoparticles and changing the circular minichannel shape on behavior of two-phase laminar mixed convection of Ag/water nanofluid, Alex. Eng. J. (2022).
[215] B. Ruhani, M.T. Andani, A.M. Abed, N. Sina, G.F. Smaisim, S.K. Hadrawi, D. Toghraie, Statistical modeling and investigation of thermal characteristics of a new nanofluid containing cerium oxide powder, Heliyon 8 (11) (2022), e11373.
[216] W. Cai, R. Sabetvand, A.M. Abed, D. Toghraie, M. Hekmatifar, A. Rahbari, G. F. Smaisim, Thermal analysis of hydration process in the vicinity of the Copper matrix using molecular dynamics simulation for application in thermal engineering, Energy Rep. 8 (2022) 7468–7475.
[217] A. Moarrefzadeh, M.R. Morovvati, S.N. Angili, G.F. Smaisim, A. Khandan, D. Toghraie, Fabrication and finite element simulation of 3D printed poly L-lactic acid scaffolds coated with alginate/carbon nanotubes for bone engineering applications, Int. J. Biol. Macromol. (2022).

[218] T. Hai, A. Abidi, L. Wang, A.M. Abed, M.Z. Mahmoud, E.M.T. El Din, G. F. Smaisim, Simulation of solar thermal panel systems with nanofluid flow and PCM for energy consumption management of buildings, J. Build. Eng. 58 (2022), 104981.
[219] G. Fadhil Smaisim, A.M. Abed, S.K. Hadrawi, A. Shamel, Parametric investigation of thermal behaviour of salt-gradient solar pool for climatic conditions, Clean Energy 6 (5) (2022) 693–704.
[220] G.F. Smaisim, M. Gholami, D. Toghraie, M. Hashemian, A.M. Abed, Numerical investigation of the flow and heat transfer of Al2O3/water nanofluid in a tube equipped with stationary and self-rotating twisted tapes, Prog. Nucl. Energy 151 (2022), 104335.
[221] Y. Jiang, G.F. Smaisim, M.Z. Mahmoud, Z. Li, H.Ş. Aybar, A.M. Abed, Simultaneous numerical investigation of the passive use of phase-change materials and the active use of a nanofluid inside a rectangular duct in the thermal management of lithium-ion batteries, J. Power Sources 541 (2022), 231610.
[222] M.W. Tian, A.M. Abed, S.R. Yan, S.M. Sajadi, M.Z. Mahmoud, H.Ş. Aybar, G. F. Smaisim, Economic cost and numerical evaluation of cooling of a cylindrical lithium-ion battery pack using air and phase change materials, J. Energy Storage 52 (2022), 104925.
[223] K.A.M. Alharbi, G.F. Smaisim, S.M. Sajadi, M.A. Fagiy, H.Ş. Aybar, S.E. Elkhatib, Numerical study of lozenge, triangular and rectangular arrangements of lithium-ion batteries in their thermal management in a cooled-air cooling system, J. Energy Storage 52 (2022), 104786.
[224] W. Wu, G.F. Smaisim, S.M. Sajadi, M.A. Fagiry, Z. Li, M.A. Shamseldin, H.Ş. Aybar, Impact of phase change material-based heatsinks on lithium-ion battery thermal management: a comprehensive review, J. Energy Storage 52 (2022), 104874.
[225] M.W. Tian, G.F. Smaisim, S.R. Yan, S.M. Sajadi, M.Z. Mahmoud, H.Ş. Aybar, A. M. Abed, Economic cost and efficiency analysis of a lithium-ion battery pack with the circular and elliptical cavities filled with phase change materials, J. Energy Storage 52 (2022), 104794.
[226] W. Brontowiyono, W.A. AbdulHussein, G.F. Smaisim, M.Z. Mahmoud, S. Singh, H. A. Lafta, S. Aravindhan, Annealing temperature effect on structural, magnetic properties and methyl green degradation of Fe2O3 nanostructures, Arabian J. Sci. Eng. (2022) 1–8.
[227] Y. Tian, I. Patra, H.S. Majdi, N. Ahmad, R. Sivaraman, G.F. Smaisim, M. Hekmatifar, Investigation of atomic behavior and pool boiling heat transfer of water/Fe nanofluid under different external heat fluxes and forces: a molecular dynamics approach, Case Stud. Therm. Eng. 38 (2022), 102308.
[228] G.F. Smaisim, H. Al-Madhhachi, A.M. Abed, Study the thermal management of Li-ion batteries using looped heat pipes with different nanofluids, Case Stud. Therm. Eng. 37 (2022), 102227.
[229] G.F. Smaisim, A.M. Abed, A. Shamel, Modeling the Thermal Performance for Different Types of Solar Chimney Power Plants, Complexity, 2022, 2022.
[230] G.F. Smaisim, M.O. Bidgoli, K.L. Goh, H. Bakhtiari, Review of thermoelastic, thermal properties and creep analysis of functionally graded cylindrical shell, Aust. J. Mech. Eng. (2022) 1–12.
[231] G.F. Smaisim, A.M. Abed, S.K. Hadrawi, A. Shamel, Modeling and thermodynamic analysis of solar collector cogeneration for residential building energy supply, J. Eng. 2022 (2022).
[232] M. Mozafarifard, A. Azimi, H. Sobhani, G.F. Smaisim, D. Toghraie, M. Rahmani, Numerical study of anomalous heat conduction in absorber plate of a solar collector using time-fractional single-phase-lag model, Case Stud. Therm. Eng. 34 (2022), 102071.
[233] Z.M. Sharba, G.F. Smaisim, A.A.A. Arani, Thermal performance of inline and staggered bank of tubes with laminar cross flow, in: 2022 5th International Conference on Engineering Technology and its Applications (IICETA), 2022, May, pp. 77–84.
[234] G.F. Smaisim, N.M. Prabu, A.P. Senthilkumar, A.M. Abed, Synthesis of biodiesel from fish processing waste by nano magnetic catalyst and its thermodynamic analysis, Case Stud. Therm. Eng. (2022), 102115.
[235] W.A. AbdulHussein, A.M. Abed, D.B. Mohammed, G.F. Smaisim, S. Baghaei, Investigation of boiling process of different fluids in microchannels and nanochannels in the presence of external electric field and external magnetic field using molecular dynamics simulation, Case Stud. Therm. Eng. (2022), 102105.
[236] S. Ahamad, M. Mohseni, V. Shekher, G.F. Smaisim, A. Tripathi, J. Alanya-Beltran, A detailed analysis of the critical role of artificial intelligence in enabling high-performance cloud computing systems, in: 2022 2nd International Conference on Advance Computing and Innovative Technologies in Engineering (ICACITE), IEEE, 2022, April, pp. 156–159.
[237] A.N. Doss, D. Shah, G.F. Smaisim, M. Olha, S. Jaiswal, A comprehensive analysis of internet of things (IOT) in enhancing data security for better system integrity-A critical analysis on the security attacks and relevant countermeasures, in: 2022 2nd International Conference on Advance Computing and Innovative Technologies in Engineering (ICACITE), IEEE, 2022, April, pp. 165–167.
[238] A. Lefteh, M. Houshmand, M. Khorrampanah, G.F. Smaisim, Optimization of modified adaptive neuro-fuzzy inference system (MANFIS) with artificial bee colony (ABC) algorithm for classification of bone cancer, in: 2022 Second International Conference on Distributed Computing and High Performance Computing (DCHPC), IEEE, 2022, March, pp. 78–81.
[239] Perforated pipe improved due to nano-fluid, J. Phys. Conf. 1 (1973), 012075 (IOP Publishing).
[240] H. Al-Madhhachi, G.F. Smaisim, Experimental and numerical investigations with environmental impacts of affordable square pyramid solar still, Sol. Energy 216 (2021) 303–314.
[241] G.F. Smaisim, Investigation on heat transfer augmentation using continuous and broken ribs on a plate of heat exchanger, Int. J. Energy Environ. 9 (3) (2018).
[242] G.F. Smaisim, Augmentation of heat transfer in corrugated tube using four-start spiral wall, Al-Qadisiya Journal for Engineering Sciences 10 (4) (2017) 451–467.
[243] G.F. Smaisim, Enhancement heat transfer of Cu-water nanofluids with thermophysical properties modeling by artificial neural network, J. Univ. Bombay 25 (5) (2017) 1721–1735.
[244] G. Smaisim, O. Fatta, A. Valera-Medina, A. Rageb, N. Syred, Investigation of heat transfer and fluid mechanics across a heated rotating circular cylinder in crossflow, in: 54th AIAA Aerospace Sciences Meeting, 2016, p. 494.
[245] G. Smaisim, O. Fatla, A. Valera Medina, A.M. Rageb, N. Syred, Experimental and theoretical investigation of the effect of rotating circular cylinder speed on the lift and drag forces, Int. J. Energy Environ. 7 (1) (2016) 23–36.
[246] S.D. Farahani, S. Mohammadi, A.D. Farahani, G.F. Smaisim, Control of the melting process in a rectangular energy storage chamber filled with phase change material in the presence of an oscillating and rotating cylinder, J. Energy Storage 60 (2023), 106628.
[247] S. Mir, A.M. Abed, O.A. Akbari, A. Mohammadian, D. Toghraie, A. Marzban, G. F. Smaisim, Effects of curvature existence, adding of nanoparticles and changing the circular minichannel shape on behavior of two-phase laminar mixed convection of Ag/water nanofluid, Alex. Eng. J. 66 (2023) 707–730.
[248] F. Wang, N. Nasajpour-Esfahani, A.A. Alizadeh, G.F. Smaisim, A.M. Abed, S. K. Hadrawi, D. Toghraie, Thermal performance of a phase change material (PCM) microcapsules containing Au nanoparticles in a nanochannel: a molecular dynamics approach, J. Mol. Liq. (2023), 121128.
[249] Y. Chen, A.A. Alizadeh, A.M. Abed, N. Nasajpour-Esfahani, G.F. Smaisim, S. K. Hadrawi, D. Toghraie, The combustion process of methyl ester-biodiesel in the presence of different nanoparticles: a molecular dynamics approach, J. Mol. Liq. (2023), 121232.
[250] M.P. Narayanasamy, G.F. Smaisim, A.M. Abed, et al., Experimental and Computational Analysis of Pin-Fin Profiles for Aerospace Applications, Iran J Sci Technol Trans Mech Eng, 2023, https://doi.org/10.1007/s40997-022-00585-y.
[251] Y. Wang, N. Nasajpour-Esfahani, A.A. Alizadeh, G.F. Smaisim, A.M. Abed, S. K. Hadrawi, M. Hekmatifar, Numerical simulation of the melting of solid paraffin in a solar water heater and the effect of the number of fins and the height of the fins, Case Stud. Therm. Eng. 41 (2023), 102653.
[252] S.D. Farahani, S. Mohammadi, A.D. Farahani, G.F. Smaisim, Control of the melting process in a rectangular energy storage chamber filled with phase change material in the presence of an oscillating and rotating cylinder, J. Energy Storage 60 (2023), 106628.
[253] S. Mir, A.M. Abed, O.A. Akbari, A. Mohammadian, D. Toghraie, A. Marzban, G. F. Smaisim, Effects of curvature existence, adding of nanoparticles and changing the circular minichannel shape on behavior of two-phase laminar mixed convection of Ag/water nanofluid, Alex. Eng. J. 66 (2023) 707–730.
[254] A. Abderrahmane, A. Mourad, S. Mohammed, G.F. Smaisim, D. Toghraie, A. Koulali, O. Younis, Second law analysis of a 3D magnetic buoyancy-driven flow of hybrid nanofluid inside a wavy cubical cavity partially filled with porous layer and non-Newtonian layer, Ann. Nucl. Energy 181 (2023), 109511.
[255] F. Wang, N. Nasajpour-Esfahani, A.A. Alizadeh, G.F. Smaisim, A.M. Abed, S. K. Hadrawi, D. Toghraie, Thermal performance of a phase change material (PCM) microcapsules containing Au nanoparticles in a nanochannel: a molecular dynamics approach, J. Mol. Liq. (2023), 121128.
[256] Y. Chen, A.A. Alizadeh, A.M. Abed, N. Nasajpour-Esfahani, G.F. Smaisim, S. K. Hadrawi, D. Toghraie, The combustion process of methyl ester-biodiesel in the presence of different nanoparticles: a molecular dynamics approach, J. Mol. Liq. (2023), 121232.
[257] M.P. Narayanasamy, G.F. Smaisim, A.M. Abed, S.L. Joseph Leon, K. Subramani, Experimental and computational analysis of pin-fin profiles for aerospace applications, Iranian Journal of Science and Technology, Transactions of Mechanical Engineering (2023) 1–11.
[258] M.M. Kadhim, A.M. Rheima, Z.S. Abbas, H.H. Jlood, S.K. Hachim, W.R. Kadhum, Evaluation of a biosensor-based graphene oxide-DNA nanohybrid for lung cancer, RSC Adv. 13 (4) (2023) 2487–2500.
[259] M.A. Mahdi, M.A. Farhan, Z.H. Mahmoud, A.M. Rheima, Z. sabri Abbas, M. M. Kadhim, A.H. Ismail, Direct sunlight photodegradation of Congo red in aqueous solution by TiO2/rGO binary system: experimental and DFT study, Arab. J. Chem. 16 (8) (2023), 104992.
[260] H. Pallathadka, H.K. Mohammed, Z.H. Mahmoud, A.A. Ramírez-Coronel, F. M. Altalbawy, M.A. Gatea, M. Kazemnejadi, Ultrasound-promoted metal-free homogenous olefins epoxidation and direct conversion of alkenes to cyclic carbonates using catalytic TAIm [X](X= WO42-, HSO5-) recyclable ionic liquid under mild conditions, Inorg. Chem. Commun. (2023), 110944.
[261] Z.H. Mahmoud, M.M. Kadhim, A.M. Rheima, Z. sabri Abbas, Z.T. Abed, F. mohamed dashoor Al-Jaafari, F.K. Ali, Functionalize and supercapacitor performance of magnetic oxide nanoparticles, Inorg. Chem. Commun. (2023), 110884.
[262] Z.H. Mahmoud, A. Hamrouni, A.B. Kareem, M.A. Mostafa, A.H. Majeed, Synthesis and characterization of chitosan sheet modified by varied weight ratio of anatase (TiO2) nano mixture with Cr (VI) adsorbing, Kuwait Journal of Science (2023).
[263] W.A. Siswanto, R.M. Romero-Parra, R. Sivaraman, A. Turki Jalil, M.A. Gatea, M. S. Alhassan, Z.H. Mahmoud, The characterization of plastic behavior and mechanical properties in the gradient nanostructured copper, Proc. Inst. Mech. Eng., Part L (2023), 14644207231161752.
[264] Z.H. Mahmoud, J.M. Mahmood, N.S. Al-Obaidi, A.M. Rahima, Gama-Fe2O3 silica-coated 2-(2-benzothiazolyl azo)-4-methoxyaniline for supercapacitive performance: original scientific paper, J. Electrochem. Sci. Eng. (2023).

[265] Z.H. Mahmoud, A.B. Mahdi, Y.S. Alnassar, H.N.K. Al-Salman, Formulation and sustained-release of verapamil hydrochloride tablets, Chemist 76 (2023).
[266] Z.H. Mahmoud, O.G. Hammoudi, A.N. Abd, Y.M. Ahmed, U.S. Altimari, A. H. Dawood, R. Shaker, Functionalize cobalt ferrite and ferric oxide by nitrogen organic compound with high supercapacitor performance, Results in Chemistry 5 (2023), 100936.
[267] S.A. Jasim, S.A.J. Ali, O.Q. Fadhil, M.K. Rakhmatova, H.H. Kzar, R. Margiana, M. Q. Sultan, Investigating the effects of hydro-alcoholic urtica dioica extract and retinoic acid on follicular development: an animal study, Med. J. Islam. Repub. Iran 37 (2023).
[268] N.S. Al-Obaidi, Z.E. Sadeq, Z.H. Mahmoud, A.N. Abd, A.S. Al-Mahdawi, F.K. Ali, Synthesis of chitosan-TiO2 nanocomposite for efficient Cr (VI) removal from contaminated wastewater sorption kinetics, thermodynamics and mechanism, J. Oleo Sci. 72 (3) (2023) 337–346.
[269] S.A. Jasim, A.H. Jabbar, D.O. Bokov, Z.I. Al Mashhadani, A. Surendar, T.Z. Taban, Y.F. Mustafa, The effects of oxide layer on the joining performance of CuZr metallic glasses, Trans. Indian Inst. Met. 76 (1) (2023) 239–247.
[270] S.A. Jasim, M.H. Ali, Z.H. Mahmood, M. Rudiansyah, F.H. Alsultany, Y. F. Mustafa, A. Surendar, Role of alloying composition on mechanical properties of CuZr metallic glasses during the nanoindentation process, Met. Mater. Int. 28 (9) (2022) 2075–2082.
[271] D.O. Bokov, Y.F. Mustafa, Z.H. Mahmoud, W. Suksatan, M.A. Jawad, T. Xu, Cr-SiNT, Mn-SiNT, Ti-C70 and Sc-cnt as effective catalysts for CO2 reduction to CH3OH, Silicon 14 (14) (2022) 8493–8503.
[272] S.A. Jasim, W.K. Abdelbasset, K. Hachem, M.M. Kadhim, G. Yasin, M.A. Obaid, Z. H. Mahmoud, Novel Gd2O3/SrFe12O19@ Schiff base chitosan (Gd/SrFe@ SBCs) nanocomposite as a novel magnetic sorbent for the removal of Pb (II) and Cd (II) ions from aqueous solution, J. Chin. Chem. Soc. 69 (7) (2022) 1079–1087.
[273] A.A. Mansoor Al Sarraf, H. Alsultany, F.H. Mahmoud, Z.S. Shafik, S. I, Z. Al, A. Sajjadi, Magnetic nanoparticles supported zinc (II) complex (Fe3O4@ SiO2-Imine/Thio-Zn (OAc) 2): a green and efficient magnetically reusable zinc nanocatalyst for synthesis of nitriles via cyanation of aryl iodides, Synth. Commun. 52 (9–10) (2022) 1245–1253.
[274] Z. Hameed Mahmood, Y. Riadi, H.A. Hammoodi, A.F. Alkaim, Y. Fakri Mustafa, Magnetic Nanoparticles Supported Copper Nanocomposite: A Highly Active Nanocatalyst for Synthesis of Benzothiazoles and Polyhydroquinolines, Polycyclic Aromatic Compounds, 2022, pp. 1–19.
[275] Z.H. Mahmoud, R.A. Al-Bayati, A.A. Khadom, The efficacy of samarium loaded titanium dioxide (Sm: TiO2) for enhanced photocatalytic removal of rhodamine B dye in natural sunlight exposure, J. Mol. Struct. 1253 (2022), 132267.
[276] I. Raya, A.A. Mansoor Al Sarraf, G. Widjaja, S. Ghazi Al-Shawi, M. F Ramadan, Z. H. Mahmood, H. Ghaleb Maabreh, ZnMoO4 nanoparticles: novel and facile synthesis, characterization, and photocatalytic performance, Journal of Nanostructures 12 (2) (2022) 446–454.
[277] Z.H. Mahmood, M. Jarosova, H.H. Kzar, P. Machek, M. Zaidi, A. Dehno Khalaji, M.M. Kadhim, Synthesis and characterization of Co3O4 nanoparticles: application as performing anode in Li-ion batteries, J. Chin. Chem. Soc. 69 (4) (2022) 657–662.
[278] A. Bahadoran, M.K. Jabarabadi, Z.H. Mahmood, D. Bokov, B.J. Janani, A. Fakhri, Quick and sensitive colorimetric detection of amino acid with functionalized-silver/copper nanoparticles in the presence of cross linker, and bacteria detection by using DNA-template nanoparticles as peroxidase activity, Spectrochim. Acta Mol. Biomol. Spectrosc. 268 (2022), 120636.
[279] Z.H. Mahmoud, R.A. Al-Bayati, A.A. Khadom, Electron transport in dye-sanitized solar cell with tin-doped titanium dioxide as photoanode materials, J. Mater. Sci. Mater. Electron. 33 (8) (2022) 5009–5023.
[280] I. Raya, G. Widjaja, Z.H. Mahmood, A.J. Kadhim, K.O. Vladimirovich, Y. F. Mustafa, L. Kafi-Ahmadi, Kinetic, isotherm, and thermodynamic studies on Cr (VI) adsorption using cellulose acetate/graphene oxide composite nanofibers, Appl. Phys. A 128 (2) (2022) 167.
[281] Z.H. Mahmoud, R.A. Al-Bayati, A.A. Khadom, In situ polymerization of polyaniline/samarium oxide-anatase titanium dioxide (PANI/Sm2O3-TiO2) nanocomposite: structure, thermal and dielectric constant supercapacitor application study, J. Oleo Sci. 71 (2) (2022) 311–319.
[282] A.M. Rheima, H.N.K. Al-Salman11, Supercapacitor performance of Fe3O4 and Fe3O4@ SiO2-bis (aminopyridine)-Cu hybrid nanocomposite, Int. J. Electrochem. Sci. 17 (221057) (2022) 2.
[283] Z.H. Mahmoud, R.A. Al-Bayati, A.A. Khadom, Synthesis and supercapacitor performance of polyaniline-titanium dioxide-samarium oxide (PANI/TiO 2-Sm 2 O 3) nanocomposite, Chem. Pap. (2022) 1–12.
[284] S. Chupradit, I. Raya, D.T. Ngoc Huy, D. Bokov, P. Van Tuan, A. Surendar, S. Sajjadifar, Role of glass composition on mechanical properties of shape memory alloy-metallic glass composites, Adv. Mater. Sci. Eng. 2021 (2021) 1–9.
[285] Z.H. Mahmoud, R.A. Al-Bayati, A.A. Khadom, Enhanced photovoltaic performance of dye-sanitized solar cell with tin doped titanium dioxide as photoanode materials, Chalcogenide Lett. 18 (12) (2021).
[286] W.J. Stępniowski, Z. Bojar, Nanoporous anodic aluminum oxide: fabrication, characterization, and applications, in: M. Aliofkhazraei, A. Makhlouf (Eds.), Handbook of Nanoelectrochemistry, Springer, Cham, 2015, https://doi.org/10.1007/978-3-319-15207-3_19-1.
[287] G.Y. Zhao, C.L. Xu, D.J. Guo, H. Li, H.L. Li, Template preparation of Pt nanowire array electrode on Ti/Si substrate for methanol electro-oxidation, Appl. Surf. Sci. 253 (2007) 3242–3246.
[288] Y. Zhang, S.J. Son, H. Ju, Anodized aluminum oxide membranes of tunable porosity with platinum nanoscale-coating for photonic application, Curr. Appl. Phys. 12 (2012) 1561–1565.
[289] R. Zhang, K.M. Jiang, D.L. Chen, G.Q. Ding, Indium oxide nanorods and nanowires on porous anodic alumina, Mater. Lett. 63 (2009) 1044–1046.
[290] L. Zhang, F. Meng, Y. Chen, J. Liu, Y. Sun, T. Luo, M. Li, J. Liu, A novel ammonia sensor based on high density, small diameter polypyrrole nanowire arrays, Sens. Actuators, B 142 (2009) 204–209.
[291] G.B. Pour, H. Ashourifar, L.F. Aval, S. Solaymani, CNTs-supercapacitors: a review of electrode nanocomposites based on CNTs, graphene, metals, and polymers, Symmetry 15 (6) (2023) 1179.
[292] A. Akbari, H. Ashourifar, G.B. Pour, K.M. Agah, A frequency-wavenumber imaging algorithm for detection of subsurface targets in layered mediums, Arabian J. Geosci. 16 (3) (2023) 163.
[293] Y.F. Avval, G.B. Pour, M.M. Aram, Fabrication of high efficiency coronavirus filter using activated carbon nanoparticles, Int. Nano Lett. 12 (4) (2022) 421–426.
[294] M. Mirzaee, M.S. Kan, G.B. Pour, Inflation and deflation of aircraft's tire with intelligent tire pressure regulation system, in: 2021 IEEE/AIAA 40th Digital Avionics Systems Conference (DASC), IEEE, 2021, October, pp. 1–6.
[295] G. Behzadi pour, H. Nazarpour fard, L. Fekri aval, P. Esmaili, Polyvinylpyridine-based electrodes: sensors and electrochemical applications, Ionics 26 (2020) 549–563.
[296] G.B. Pour, L.F. Aval, M. Mirzaee, CNTs supercapacitor based on the PVDF/PVA gel electrolytes, Recent Pat. Nanotechnol. 14 (2) (2020) 163–170.
[297] L.F. Aval, Influence of oxide film surface morphology and thickness on the properties of gas sensitive nanostructure sensor, Indian J. Pure Appl. Phys. 57 (10) (2019) 743–749.
[298] H. Ashourifar, K. Mikaili Agah, G. Behzadi Pour, A. Akbari, S.A. Sebt, The effect of electron flow on coercivity and remanence of FePt nanocomposites under heat treatment, J. Supercond. Nov. Magnetism 32 (2019) 3339–3343.
[299] G. Behzadi Pour, L. Fekri Aval, P. Esmaili, Performance of gas nanosensor in 1-4 per cent hydrogen concentration, Sens. Rev. 39 (4) (2019) 622–628.
[300] M. Mirzaee, G.B. Pour, Design and fabrication of ultracapacitor based on paper substrate and BaTiO3/PEDOT: PSS separator film, Recent Pat. Nanotechnol. 12 (3) (2018) 192–199.
[301] S. Khatami, L. Fekri Aval, G. Behzadi Pour, Investigation of nanostructure and optical properties of flexible AZO thin films at different powers of RF magnetron sputtering, Nano 13 (6) (2018), 1850062.
[302] G. Behzadi Pour, Electrical properties of the MOS capacitor hydrogen sensor based on the Ni/SiO2/Si structure, J. Nanoelectron. Optoelectron. 12 (2) (2017) 130–135.
[303] G. Behzadi, L. Fekri, Electrical parameter and permittivity measurement of water samples using the capacitive sensor, International Journal of Water Resources and Environmental Sciences 2 (3) (2013) 66–75.
[304] G. Behzadi, L. Fekri, H. Golnabi, Effect of the reactance term on the charge/discharge electrical measurements using cylindrical capacitive probes, J. Appl. Sci. 11 (18) (2011) 3293–3300.
[305] A. Rauf, M. Mehmood, M. Ahmed, M. ul Hasan, M. Aslam, Effects of ordering quality of the pores on the photoluminescence of porous anodic alumina prepared in oxalic acid, J. Lumin. 130 (2010) 792–800.
[306] R. Mangu, S. Rajaputra, P. Clore, D. Qian, R. Andrews, V.P. Singh, Ammonia sensing properties of multiwalled carbon nanotubes embedded in porous alumina templates, Mater. Sci. Eng., B 174 (2010) 2–8.
[307] X. Zhou, H. Habazaki, K. Shimizu, P. Skeldon, G.E. Thompson, G.C. Wood, Enrichmentdependent anodic oxidation of zinc in Al–Zn alloys, Corrosion Sci. 38 (1996), 1563–157.
[308] T. Kondo, K. Nishio, H. Masuda, Fabrication of Au fine structures of nanoparticles by anodization of purple gold (AuAl2), Chem. Lett. 38 (2009) 1148–1149.
[309] A. Yin, R.S. Guico, J. Xu, Fabrication of anodic aluminium oxide templates on curved surfaces, Nanotechnology 18 (3) (2007), 035304.